Original Investigation

Diagnosis of Regional Node Metastases in Lung Cancer with Computer-Aided 3D Measurement of the Volume and CT-Attenuation Values of Lymph Nodes

Yoshiyuki Takahashi, Shodayu Takashima, MD, PhD, Tomoaki Hakucho, Chie Miyake, Daisuke Morimoto, Bing-hu Jiang, Hodaka Numasaki, MS, Yasuhiko Tomita, MD, Katsuyuki Nakanishi, MD, Masahiko Higashiyama, MD

Rationale and Objectives: The aim of this study is to assess the usefulness of computer-aided three-dimensional (3D) measurement of volume and computed tomography (CT) attenuation values of nodes for diagnosing nodal metastases of lung cancer.

Materials and Methods: We measured three diameters, their ratios, volume, and CT values in 3D images of 191 nodes (64 malignant; 162 of <1 cm in short diameter) in 26 consecutive patients who underwent contrast-enhanced, thin-section, multidetector row CT before surgery. We separately studied statistically significant factors in a group of all nodes and in another group of nodes of <1 cm in short diameter with logistic modeling and evaluated their diagnostic accuracy.

Results: Significant factors were CT values ($P < .001$) and short diameter ($P = .001$) for the total node group, and CT values ($P = .030$) and 3D volume ($P = .035$) for the <1 cm node group. Optimal 83% accuracy was obtained with a criterion of short diameter of >7.4 mm and CT values of >103 Hounsfield unit (HU) for the total node group, whereas optimal 76% accuracy was obtained with a criterion of 3D volume of >1282 mm^3 or CT values of >103 HU for the <1 cm node group.

Conclusion: 3D measurement may be useful for diagnosing nodal metastases.

Key Words: Lung cancer; 3D measurement; computer-aided diagnosis; lymph node metastasis; 3D volume.

Non–small-cell lung cancer (NSCLC) is staged based on the TNM classification system, because appropriate therapy depends on the staging of cancer as determined by this system and because prognosis of patients correlates well with the staging of NSCLC (1). Presence or absence of lymph node metastasis and its site (N-staging) are one of the three major factors of TNM system. Overall survival rates decrease as N-staging of NSCLC advances; a 5-year survival rate (56%) of patients with pathological N0 (pN0) disease was significantly better than that (38%) with pN1 disease, which was significantly better than that (22%) with pN2 disease (2).

Although various noninvasive and (semi)invasive procedures are used for staging NSCLC, computed tomography (CT) is initially employed and a widely used imaging technique for this purpose (3,4). Diagnosis with CT of nodal metastasis in NSCLC depends only on the diameters of nodes in two-dimensional images; at present, transverse short diameter of 1 cm is generally adopted for prediction of nodal metastasis (3,4). However, a meta-analysis reported poor sensitivity of 51% with 86% specificity of CT for identifying mediastinal node metastasis (3). To our knowledge, there is no literature in which three-dimensional (3D) measurements with computer-aided volume and CT attenuation values of regional nodes were applied to predict nodal metastasis in NSCLC.

In the current study, we retrospectively evaluated the usefulness of computer-aided 3D measurements of volume and CT-attenuation values of lymph nodes on intravenous (IV) contrast-enhanced thin-section multidetector row CT (MDCT) for diagnosis of nodal metastasis in NSCLC.

Acad Radiol 2013; ■:1–6

From the Osaka University Graduate School of Medicine, Division of Allied Health Sciences, Department of Diagnostic Radiological Imaging, 1-7 Yamadaoka, Suita, Osaka 565-0871, Japan (Y.T., S.T., T.H., C.M., D.M., B.-h.J., H.N.); Osaka Medical Center for Cancer and Cardiovascular Diseases, Osaka, Japan (Y.T., K.N., M.H.). Received October 15, 2012; accepted January 30, 2013. **Address correspondence to:** Y.T. e-mail: yoshi_seat_128@yahoo.co.jp

http://dx.doi.org/10.1016/j.acra.2013.01.013

MATERIALS AND METHODS

Patient and CT Technique

This study was approved by an institutional review board. Between June 2006 and October 2008, 206 patients with T1 lung cancer underwent surgical resection of primary tumor with dissection of regional lymph nodes in our hospital. Of these, 180 patients (87% of 206) proved not to have regional node metastases in subsequent pathologic diagnoses. Thus, the current series included 26 consecutive patients with T1 lung cancer (tumor histology: 23 adenocarcinoma and 3 squamous cell carcinoma; mean age, 63 ± 10 years; 20 men and 6 women; body weight, 60–80 kg) who had pathologically verified metastases in the ipsilateral hilar or mediastinal nodes or subcarinal nodes and had contrast-enhanced thin-section CT before surgery in our hospital.

Written informed consent for CT was obtained from all patients. Contrast-enhanced thin-section CT scans were acquired through chest and upper abdomen with a 16 detector row CT (Aqulion16, Toshiba, Tokyo, Japan) using the following CT parameters: X-ray tube voltage of 120 kV, tube current of 150–250 mA, field of view of 35 cm, collimation of 0.5 mm, helical pitch of 1.5, and acquisition time of 0.5 seconds per rotation. A total of 100 mL (300 mg I/mL) of contrast media (iopamidol, Iopamiron 300; Bayer Healthcare) was IV injected with a rate of 2 mL/second and a time delay of 40 seconds with use of a power injector (Dual Shot GX; Nemoto Kyorindo, Tokyo, Japan). Chest CT images were reconstructed with lung kernel.

Image Analysis

A radiation technologist (Y.T.), in concert with a chest radiologist (S.T.; 25 years' experience in chest radiology), carried out all the following analyses with computer assistance. They selected all of the nodes of >3 mm in short diameter on CT images that were located in the same hemithorax as the primary tumor or in the subcarinal region because of technical limitations in segmentation of lymph nodes; they also constructed 3D images of the nodes semiautomatically with computer assistance (Fig 1). Conglomerated nodes were excluded from the current assessment, because these nodes can cause inaccuracy in node-by-node comparison study.

Operation and analysis of all CT images were performed using in-house programmed software that was installed on a commercially available workstation (Virtual Place, MI Lab, Tokyo, Japan). In this software, the lymph nodes were isolated from other tissues and structures using an automatic threshold technique. Manual operation was required to separate lymph nodes from adjacent structures, such as vessels and bronchi. They measured greatest and transverse short diameter, greatest vertical diameter, ratios of transverse short to greatest, transverse greatest to vertical, and transverse short to vertical diameters, 3D volume, and 3D CT-attenuation values of the nodes. They measured CT values of all voxels of the nodes, manually excluding the areas of apparent necrosis, calcification, fat, or large vessels and used mean CT-attenuation values for analysis.

Time intervals between CT studies and surgery ranged from 7 to 29 days with mean interval of 16 days. Dissected nodes were subdivided into 14 anatomical compartments according to the nodal mapping nomenclature and submitted them for pathological examinations (2). Submitted nodes were fixed in formalin, cut in the greatest dimensions of the nodes, sliced, and stained with hematoxylin & eosin. Surgically resected nodes that corresponded to the CT images were determined by the consensus of the radiologist and pathologist (Y.T.; 20 years' experience in diagnostic pathology) based on the anatomical location, diameters, and shape of the nodes. Thus, node-by-node comparison between CT images and pathologic diagnosis of nodal metastasis was made retrospectively. In this study, we first made node-by-node comparison in metastatic nodes and then the other nodes were regarded as benign, because lymph node dissection was carried out in all patients. Beforehand, we examined the difference in greatest transverse diameters of 20 nodes between CT images and pathologic specimens. This preliminary study revealed that the diameters of pathologic specimens were 2% smaller than the CT images on average.

Statistical Analysis

We studied statistically significant differences between benign and malignant nodes for each factor and performed stepwise logistic modeling using all statistically significant factors as independent variables to determine the most useful factors for diagnosing nodal metastases; we then calculated diagnostic accuracy with use of the optimal parameters. We carried out those statistical analyses separately in a group of all nodes and in another group of nodes of <1 cm in short diameter.

Next, we used receiver operating characteristic (ROC) technique to evaluate diagnostic capability of each statistically significant factor determined with logistic modeling. Then, we performed stepwise multiple regression analyses in all of the nodes to evaluate correlation between 3D volume of nodes and three diameters (transverse greatest and short diameter, greatest vertical diameter of nodes). Finally, we compared diagnostic capability for N-staging between the traditional size criterion (≥1 cm in transverse short diameter of nodes) and the optimal criterion proposed in the current study. Student's *t*-test was used for comparison of the means of each pair. We calculated Pearson correlation coefficients to estimate correlation between a pair of data. A P value less than .05 was considered to indicate a statistically significant difference. All of the statistical calculations were performed using SPSS software (SPSS, Chicago, IL).

RESULTS

A total of 473 nodes were dissected. Of these, 306 nodes were in the mediastinum or hilum and an average of 3.1 nodes

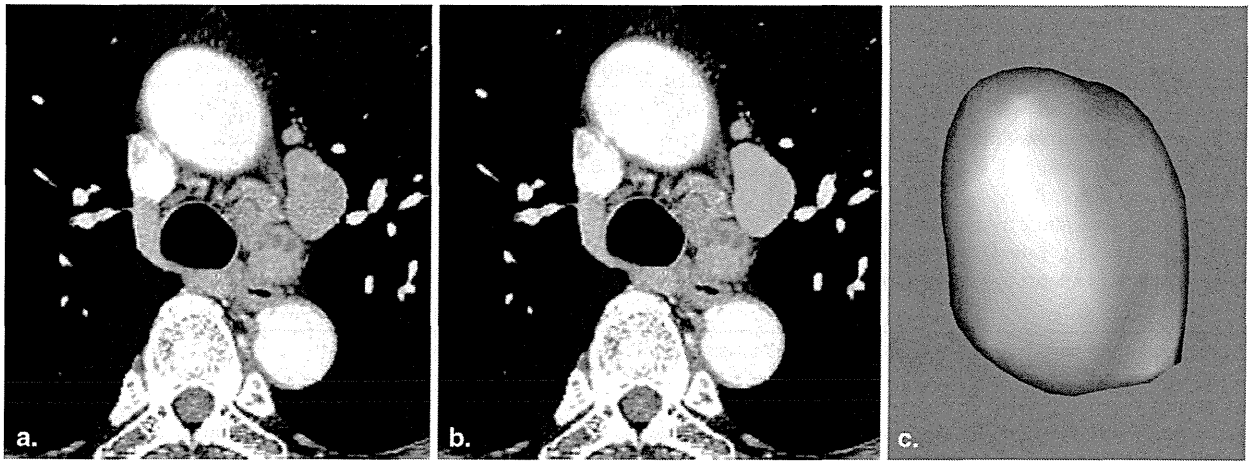

Figure 1. Methods of segmentation and three-dimensional (3D) measurement of mediastinal lymph nodes in a 61-year-old man with adenocarcinoma in the left lung. **(a)** Intravenous contrast-enhanced thin-section computed tomography (CT) demonstrated multiple lymph nodes in #4L, #5, and #6. **(b)** Swollen node (*green color*) in #5 was semiautomatically segmented from surrounding structures with computer assistance. CT attenuation values and areas of the node in transverse plane were automatically calculated. Greatest and shortest diameters in transverse plane were also measured. **(c)** Surface rendering 3D image of segmented node was depicted. Mean CT attenuation values and volume of the node were automatically calculated with computer assistance. Greatest vertical diameter was also measured.

(range 1–8) per nodal region in the mediastinum or hilum was removed. In pathologic studies, there were 85 metastatic nodes (2 nodes in region 1, 2 in region 2, 8 in region 3, 12 in region 4, 7 in region 5, 2 in region 6, 14 in region 7, and 38 in region 10). According to pathologic N staging, 8 patients were staged as N1 disease and 18 as N2 disease. Of the 85 nodes, 64 nodes (75%) were visualized on CT images as nodes of >3 mm in short diameter in the corresponding anatomical compartments; the remaining 21 nodes (25%) were not identified or depicted as nodes of ≤3 mm in short diameter on CT images.

Of the 64 metastatic nodes, 50 nodes (78%) were in nodal regions, of which number of dissection was 3 or less. Although the remaining 14 metastatic nodes were in nodal regions of which number of dissection was more than 3 (range 4–8), diagnosis of metastasis was reliably made based on the meticulous comparison of dimensions and shape of the nodes. In CT imaging, 191 nodes in 26 patients were segmented from the surrounding tissues and were available for CT analyses. Thus, CT-pathologic correlation was carried out in the 191 nodes (127 benign, 64 malignant). Of these, 12 nodes showed foci of necrosis, fat deposits, or calcification on CT images. Of the 191 nodes, 162 (85%; 119 benign, 43 malignant) were less than 1 cm.

Mean time for the entire segmentation and performing all measurements per node was 10 minutes with a range from 5–20 minutes. A statistically significant difference was seen in six factors (transverse greatest diameter, transverse short diameter, and vertical diameter of node, 3D volume of node, ratios of transverse short to greatest diameter of node, CT-attenuation value of node) for the total node group and in five factors (transverse short diameter, ratios of transverse short to greatest diameter and transverse short to vertical diameter, 3D volume, CT-attenuation value of node) for the <1 cm node group (Tables 1 and 2). Logistic modeling revealed the significant factors were CT-attenuation values ($P = .001$) and transverse short diameter ($P < .001$) for the total node group and CT-attenuation values ($P = .030$) and 3D volume ($P = .035$) for the <1 cm node group.

The area under the ROC curves for CT-attenuation values and transverse short diameter in the total node group was 0.68 ± 0.04 (standard error of the mean) and 0.80 ± 0.03, respectively, whereas the area under the ROC curves for CT-attenuation values and 3D volume in the <1 cm node group was 0.64 ± 0.05 and 0.61 ± 0.05, respectively.

Stepwise multiple regression analyses in the total node group revealed that all the three diameters had a significant correlation with 3D volume. A standardized partial regression coefficient was 0.40 for transverse short diameter ($P < .001$), 0.29 for transverse greatest diameter ($P < .001$), and 0.26 for vertical greatest diameter ($P < .001$).

For the total node group, optimal 83% accuracy with 67% sensitivity and 91% specificity for predicting metastatic nodes was obtained with a criterion of transverse short diameter of >7.4 mm or CT-attenuation values of >102 Hounsfield units (HU) (Table 3). Using the single parameters, transverse short diameter of >11.4 invariably indicated metastasis, and CT-attenuation values of >123 HU were specific to nodal metastasis. With use of the combined criteria, transverse short diameter of >7.4 mm and CT-attenuation values of >102 HU were specific to nodal metastasis.

Regarding the <1 cm node group, optimal 76% accuracy with 18% sensitivity and 97% specificity was obtained with a criterion of 3D volume of >1282 mm^3 or CT-attenuation values of >102 HU (Table 4). Using the single parameters, 3D volume of >1960 mm^3 invariably indicated metastasis and CT-attenuation values of >126 HU were specific to nodal

TABLE 1. Comparison of Eight Measurement Results in CT Images between Benign and Metastatic Nodes in the Total Node Group

Factors (Mean ± SD)	Benign (*n* = 127)	Malignant (*n* = 64)	*P*
Transverse greatest diameter (mm)	10.2 ± 3.1	12.5 ± 4.2	<.001
Transverse short diameter (mm)	6.1 ± 1.8	8.7 ± 2.9	<.001
Vertical diameter (mm)	11.8 ± 3.9	15.5 ± 7.5	<.001
Volume of nodes (mm^3)	434 ± 348	1,047 ± 1,495	.002
Ratio of transverse short to greatest diameter	.64 ± .19	.72 ± .17	.005
Ratio of transverse greatest to vertical diameter	.92 ± .30	.90 ± .30	NS
Ratio of transverse short to vertical diameter	.57 ± .23	.63 ± .23	NS
CT value (HU)	.64 ± .25	.79 ± .23	<.001

CT, computed tomography; HU, Hounsfield unit; NS, not significant; SD, standard deviation.

TABLE 2. Comparison of Eight Measurement Results in CT Images between Benign and Metastatic Nodes in the <1 cm Node Group

Factors (Mean ± SD)	Benign (*n* = 119)	Malignant (*n* = 43)	*P*
Transverse greatest diameter (mm)	10.0 ± 3.0	10.9 ± 2.9	NS
Transverse short diameter (mm)	5.9 ± 1.4	7.2 ± 1.2	<.001
Vertical diameter (mm)	11.6 ± 3.7	12.5 ± 5.5	NS
Volume of nodes (mm^3)	388 ± 269	490 ± 345	.042
Ratio of transverse short to greatest diameter	.62 ± .18	.69 ± .18	.027
Ratio of transverse greatest to vertical diameter	.91 ± .31	.94 ± .29	NS
Ratio of transverse short to vertical diameter	.55 ± .20	.64 ± .21	.024
CT value (HU)	.64 ± .25	.77 ± .25	.005

CT, computed tomography; HU, Hounsfield unit; NS, not significant; SD, standard deviation.

TABLE 3. Diagnostic Statistics of Two Significant Factors for Predicting Metastatic Node Determined with Logistic Modeling in the Total Node Group

Factors	Sensitivity (%)	Accuracy (%)	Specificity (%)
Transverse short diameter (mm)			
>4.4	100	43	15
>7.4	61	74	81
>9.9	32	94	73
>11.4	13	71	100
CT value (HU)			
>4	100	35	2
>102	14	69	97
>123	3	68	100
Transverse short diameter of >7.4 mm and CT value of >102 HU	8	69	100
Transverse short diameter of >7.4 mm or CT value of >102 HU	67	83	91

CT, computed tomography; HU, Hounsfield unit.

TABLE 4. Diagnostic Statistics of two Significant Factors for Predicting Metastatic node Determined with Logistic Modeling in the <1 cm Node Group

Factors	Sensitivity (%)	Accuracy (%)	Specificity (%)
Volume of nodes (mm^3)			
>484	100	30	4
>1282	5	74	99
>1960	0	73	100
CT value (HU)			
>4	100	27	2
>102	16	75	97
>123	0	73	100
Nodal volume of >1282 mm^3 and CT value of >102 HU	2	74	100
Nodal volume of >1282 mm^3 or CT value of >102 HU	18	76	97

CT, computed tomography; HU, Hounsfield unit.

metastasis. With use of the combined criterion, 3D volume of >1282 mm^3 and CT-attenuation values of >102 HU were specific to nodal metastasis.

Sensitivity (77%, 20 of 26 patients) of our optimal criterion (transverse short diameter of >7.4 mm or CT-attenuation values of >102 HU) for predicting nodal metastasis per patient was better than that (54%, 14 of 26) of traditional criterion (≥1 cm in transverse short diameter). As for diagnosis of specific N-staging (N0, N1, or N2), the proportion of correct staging was greater for our optimal criterion (62%, 16 of 26 patients) than for the traditional one (46%, 12 out of 26 patients); overstaged patients were 2 (8%) for the traditional criterion and 3 (12%) for our optimal one because of the presence of reactive nodes, whereas understaged patients were 12 (46%) for the traditional criterion and 7 (27%) for our optimal one.

DISCUSSION

In our study, 49% of the 85 metastatic nodes were missed with CT, because they were normal-sized but had metastatic tumor. A meta-analysis of CT diagnosis of metastatic nodes in lung cancer revealed that pooled sensitivity was 51% with 95% confidence intervals (CIs) of 47% to 54%, which means 49% of the metastatic nodes on average will be missed with CT (3). Microscopic metastasis in normal-sized nodes is reported to occur in 7% to 21% of patients with lung cancer (5,6). However, its incidence depends on the histology. Many researchers have documented that adenocarcinoma showed more aggressive behavior and therefore had higher incidence of occult metastasis than other tumors such as squamous cell carcinoma (7–9). In our series, adenocarcinoma comprised the majority of lung cancer (88%), of which proportion is considerably higher than that (25%–71%) in the other reports (6–10). Thus, we think that the high proportion of adenocarcinoma is the main reason for the high incidence of occult metastasis in our series. In the same vein, biased cancer histology in our study may explain the low sensitivity (32%) of the traditional size criterion for diagnosis of nodal metastasis.

Our 3D analysis of lymph nodes demonstrated that metastatic nodes expanded three dimensionally with a resultant significant increase in the volume and became spherical in shape. Overall, increase in the nodal volume was most intimately reflected in the transverse short diameter and the tendency of spherical shape was more strongly manifested in the <1 cm nodes. In two-dimensional (2D) metric analysis of cervical nodes in head and neck cancer, several authors have stated that the ratio of transverse short to greatest diameters was useful for predicting metastatic nodes and that lymph nodes became rounded when they were involved with metastatic tumor (11,12). However, to our knowledge, no literature addressed the 3D appearance and volumetric analysis of metastatic nodes of lung cancer.

Among the various metric data assessed with multivariate analysis in the current study, a significant factor for diagnosing malignancy was a transverse short diameter for all nodes and nodal volume for the <1 cm nodes. The usefulness of transverse short diameter for predicting metastasis of lung cancer is compatible with the prior report (3). However, 3D nodal volume is a new finding on prediction of occult nodal metastasis. Puesken et al (13) reported in a comparative study of 2D and semiautomated 3D measurements of MDCT data that volumetric analysis of lymph node was superior to traditional 2D measurements for predicting nodes involved with malignant lymphoma. In another study of nodal metastasis of malignant melanoma, Fabel et al (14) demonstrated that semiautomated volumetric analysis of lymph nodes was a feasible method in therapy monitoring because interobserver variability was significantly lower in volumetric analysis than in 2D measurements of diameters of lymph nodes.

This study demonstrated that the mean CT attenuation values of lymph nodes obtained with 3D volumetric data were a significant factor for predicting both overall nodal metastasis and occult metastasis in normal-sized lymph nodes. Many investigators elucidated the role of enhancement extent obtained with dynamic enhanced CT and first-pass perfusion CT for discrimination between benign and malignant pulmonary nodules. However, no study has applied those procedures to diagnosis of nodal metastasis of lung cancer (15–18).

Yi et al (16) reported in a study of IV dynamic enhanced MDCT that the peak enhancement of the nodules was seen 103-119 seconds (range, 40-180 seconds) after IV contrast material injection and that 78% accuracy with 99% sensitivity and 54% specificity for predicting malignant pulmonary nodule was obtained with a cutoff value of ≥30 HU of net enhancement. The authors also mentioned that extent of enhancement reflected underlying nodule angiogenesis (16). A significant correlation between enhancement effect and angiogenesis of tumor was reported by many other authorities (15–17).

In the analysis of contrast-material dynamics in perfusion CT, the first pass of IV-injected contrast material occurs during the first 45–60 seconds after IV injection, which reflects predominantly perfusion and intravascular blood volume (19). The peak enhancement and the extent of enhancement of nodes were not evaluated in our series. According to our CT protocol, however, all of the nodes were imaged between 40 and 60 seconds after IV injection of contrast material. In the literature, CT values on nonenhanced CT images were not significantly different between malignant and benign pulmonary nodules (16). Some lymph nodes in an individual with aluminum pneumoconiosis are reported to show diffuse increased attenuation value on unenhanced CT (20). However, no patients in our series had such occupation history. Thus, we think that CT values of nodes on contrast-enhanced CT images will reflect the extent of enhancement in the first pass and therefore may represent intravascular blood volume of nodes.

In our study, a combined criterion of transverse short diameter of >7.4 mm and CT value of >102 HU showed an optimal accuracy of 83% with 67% sensitivity and 91% specificity for predicting metastasis of overall nodes. The diagnostic capability was better than that for the traditional size criterion, of which sensitivity and specificity were reported as 51% (95% CIs, 47%–54%) and 86% (95% CIs, 84%–88%), respectively (3). Furthermore, promising results for predicting occult metastasis were obtained with 3D nodal volume and CT values. This optimal criterion of nodal volume of >1282 mm^3 or CT values of >102 HU was highly specific (97% specificity). However, its sensitivity (18%) was too poor for clinical usage.

Our study had several limitations. First, patient population was too small to draw a conclusion, and this study was a preliminary one. Second, our study included only patients who had nodal metastasis and excluded patients who had no nodal metastasis. This can result in the sampling bias by enriching patient population for lymph node metastasis. Third, only two investigators were involved in our study; therefore, we couldn't address observer variability. Fourth, degree of

enhancement can be affected by body weight in addition to the amount of contrast media (21). However, a fixed amount of contrast media was injected in the current study, which made our thresholds of CT attenuation values for predicting metastatic nodes less useful for clinical usage. Last, we took a considerably longer time (10 minutes per node) for the entire segmentation of a node than the other researchers (57–65 seconds per node), because we used originally developed software for preclinical use only (14).

In conclusion, computer-aided 3D analysis of volume and CT attenuation values of nodes may be useful for predicting metastasis, especially occult nodal metastasis in lung cancer.

REFERENCES

1. Groome PA, Bolejack V, Crowley JJ, et al. The IASLC Lung Cancer Staging Project: validation of the proposals for revision of the T, N, and M descriptors and consequent stage groupings in the forthcoming (seventh) edition of the TNM classification of malignant tumours. J Thorac Oncol 2007; 2: 694–705.
2. Rusch VW, Crowley J, Giroux DJ, et al. The IASLC Lung Cancer Staging Project: proposals for the revision of the N descriptors in the forthcoming seventh edition of the TNM classification for lung cancer. J Thorac Oncol 2007; 2:603–612.
3. Silvestri GA, Gould MK, Margolis ML, et al. Noninvasive staging of non-small cell lung cancer: ACCP evidenced-based clinical practice guidelines (2nd edition). Chest 2007; 132:178S–201S.
4. Vansteenkiste J, Dooms C, De Leyn P. Early stage non-small-cell lung cancer: challenges in staging and adjuvant treatment: evidence-based staging. Ann Oncol 2010; 21:189–195.
5. Gross BH, Glazer GM, Orringer MB, et al. Bronchogenic carcinoma metastatic to normal-sized lymph nodes: frequency and significance. Radiology 1988; 166:71–74.
6. Arita T, Kuramitsu T, Kawamura M, et al. Bronchogenic carcinoma: incidence of metastases to normal sized lymph nodes. Thorax 1995; 50: 1267–1269.
7. Kamiyoshihara M, Kawashima O, Ishikawa S, et al. Mediastinal lymph node evaluation by computed tomographic scan in lung cancer. J Cardiovasc Surg 2001; 42:119–124.
8. Suzuki K, Nagai K, Yoshida J, et al. Clinical predictors of N2 disease in the setting of a negative computed tomographic scan in patients with lung cancer. J Thorac Cardiovasc Surg 1999; 117:593–598.
9. Funakoshi Y, Maeda H, Takeda S, et al. Tumor histology affects the accuracy of clinical evaluative staging in primary lung cancer. Lung Cancer 2010; 70:195–199.
10. Kerr KM, Lamb D, Wathen CG, et al. Pathological assessment of mediastinal lymph nodes in lung cancer: implications for non-invasive mediastinal staging. Thorax 1992; 47:337–341.
11. Takashima S, Sone S, Nomura N, et al. Nonpalpable lymph nodes of the neck: assessment with US and US-guided fine-needle aspiration biopsy. J Clin Ultrasound 1997; 25:283–292.
12. Steinkamp HJ, Hosten N, Richter C, et al. Enlarged cervical lymph nodes at helical CT. Radiology 1994; 191:795–798.
13. Puesken M, Buerke B, Gerss J, et al. Prediction of lymph node manifestations in malignant lymphoma: significant role of volumetric compared with established metric lymph node analysis in multislice computed tomography. J Comput Assist Tomogr 2010; 34:564–569.
14. Fabel M, von Tengg-Kobligk H, Giesel FL, et al. Semi-automated volumetric analysis of lymph node metastases in patients with malignant melanoma stage III/IV–a feasibility study. Eur Radiol 2008; 18:1114–1122.
15. Swensen SJ, Viggiano RW, Midthun DE, et al. Lung nodule enhancement at CT: multicenter study. Radiology 2000; 214:73–80.
16. Yi CA, Lee KS, Kim EA, et al. Solitary pulmonary nodules: dynamic enhanced multi-detector row CT study and comparison with vascular endothelial growth factor and microvessel density. Radiology 2004; 233:191–199.
17. Li Y, Yang ZG, Chen TW, et al. Peripheral lung carcinoma: correlation of angiogenesis and first-pass perfusion parameters of 64-detector row CT. Lung Cancer 2008; 61:44–53.
18. Ohno Y, Koyama H, Matsumoto K, et al. Differentiation of malignant and benign pulmonary nodules with quantitative first-pass 320-detector row perfusion CT versus FDG PET/CT. Radiology 2011; 258:599–609.
19. Miles KA. Perfusion CT for the assessment of tumour vascularity: which protocol? Br J Radiol 2003; 76:S36–S42.
20. Vahlensieck M, Overlack A, Muller KM. Computed tomographic high-attenuation mediastinal lymph nodes after aluminum exposition. Eur Radiol 2000; 10:1945–1946.
21. Brink JJA. Use of high concentration contrast media (HCCM): principles and rationale-body CT. Eur J Radiol 2003; 45:S53–S58.

Original article

F18-FDG PET-CT analyses of small peripheral adenocarcinoma of the lung

Yoshiyuki Takahashi[1], Shodayu Takashima[1], Shinichiro Watanabe[2], Yasuhiko Tomita[3], Tomoaki Hakucho[1], Chie Miyake[1], Daisuke Morimoto[1], Takuya Hosoki[4], Katsuyuki Nakanishi[3] and Masahiko Higashiyama[3]

[1]Osaka University Graduate School of Medicine, Division of Allied Health Sciences, Department of Diagnostic Radiological Imaging, Osaka; [2]Osaka University Graduate School of Medicine, Department of Nuclear Medicine and Tracer Kinetics, Osaka; [3]Osaka Medical Center for Cancer and Cardiovascular Diseases, Osaka; [4]Morinomiya Clinic, Osaka, Japan
Correspondence to: Yoshiyuki Takahashi. Email: yoshi_seat_128@yahoo.co.jp

Abstract

Background: Radiological discrimination of histologic subtypes of small peripheral adenocarcinoma of the lung is clinically important. Although there are many articles in which CT findings were used for this purpose, there are only a few reports on the capability of FDG PET-CT findings for histologic classification of this tumor.

Purpose: To investigate the correlation between visual assessment or maximum standard uptake values (SUV_{max}) on F18-FDG PET-CT and histology grading of small peripheral adenocarcinoma of the lung.

Material and Methods: Proportions of positive PET-CT diagnoses and SUV_{max} were retrospectively reviewed on 96 solitary pulmonary nodules of $\leq$2 cm in 90 consecutive patients. Tumors were classified into four groups according to Noguchi's classification (group 1 [$n = 10$], atypical adenomatous hyperplasia and type A tumors; group 2 [$n = 12$], type B tumors; group 3 [$n = 42$], type C tumors; group 4 [$n = 32$], types D, E, and F tumors). Proportions of positive PET-CT diagnoses and mean SUV_{max} of lesions among four groups were compared using trend tests to examine if there is a significant linear correlation with the progression of the histology grading of tumors. Then, an optimal threshold of SUV_{max} was proposed to best discriminate tumors of poor (groups 3 and 4) from good (groups 1 and 2) prognosis.

Results: There was a significant linear trend for both visual assessment ($P < 0.01$) and SUV_{max} ($P < 0.01$). A SUV_{max} of 0.42 showed the highest accuracy of 84% with 95% sensitivity and 50% specificity for predicting tumors of poor prognosis. A SUV_{max} of 2.05 showed 100% specificity with 49% sensitivity, and 60% accuracy. Positive visual diagnoses showed accuracy of 83% with 90% sensitivity and 59% specificity.

Conclusion: Visual assessment and SUV_{max} on PET-CT correlated well with the histology grading of small peripheral adenocarcinoma of the lung.

Keywords: PET-CT, lung cancer, lung adenocarcinoma, SUV_{max}

Submitted February 23, 2012; accepted for publication September 14, 2012

Lung cancer is the most common cancer in the world and the leading cause of cancer deaths in industrialized countries. According to the most recent global cancer statistics in 2010, lung cancer is the most common and the leading cause of cancer death in both men and women (1). Regarding the histology of lung cancer, a notable shift has recently occurred in the incidence rates of histologic subtypes of lung cancer. After steady increase in incidence since 1973, adenocarcinoma (30.7% of all cases) has replaced squamous cell carcinoma (30%) as the most frequent histologic subtype of lung cancer in the latest two decades (2). This overall increase of adenocarcinomas is largely due to a dramatic increase in adenocarcinomas with pure lepidic growth (formerly bronchioalveolar carcinoma [BAC]).

Noguchi *et al.* (3) classified peripheral adenocarcinoma of the lung of $\leq$2 cm into six types A–F based on the tumor growth pattern and demonstrated that this tumor classification correlated well with the prognosis of the tumors.

Among the subtypes, types A, B, and C tumors showed a lepidic tumor growth, whereas types D, E, and F demonstrated a destructive tumor growth. The researchers reported that the prognosis of cases of types A and B tumors (solitary adenocarcinomas with pure lepidic growth, formerly localized BAC) with a 5-year survival rate of 100% was significantly better than cases of type C tumors (adenocarcinoma with tumor components of lepidic growth) with 5-year survival rate of 75% and the prognosis of cases of type D was worst. Based on those results, T1 tumor ($\leq$3 cm) has become to be subdivided into T1a ($\leq$2 cm) and T1b (>2 cm but $\leq$3 cm) in the latest TNM classification of UICC (4).

There are many studies in which high-resolution CT findings were correlated with the histologic subtypes of peripheral adenocarcinoma of the lung defined by Noguchi *et al.* (5, 6). However, there are only a few reports on the relationship of fluorine 18-fluoro-2-deoxyglucose positron emission tomography CT (F18-FDG PET-CT) with this tumor classification (7, 8). In this study, we investigated if visual assessment and maximum standard uptake values (SUV_{max}) on PET-CT may correlate with the histology grading of small peripheral adenocarcinoma of the lung.

Material and Methods

Patients

Ninety consecutive patients (48 men and 42 women; mean age, 65 $\pm$ 10 [SD] years; range, 30–82 years) who had surgical resection of lung neoplasms from June 2006 to December 2008 were included in this study. There were 96 lesions (three of atypical adenomatous hyperplasias [AAH], seven type A tumors [adenocarcinoma with pure lepidic growth], 12 type B tumors [adenocarcinoma with lepidic growth accompanied by foci of collapse of alveolar structure], 42 type C tumors [invasive adenocarcinoma with lepidic growth], 10 type D tumors [poorly differentiated adenocarcinoma], 10 type E tumors [tubular adenocarcinoma], and 12 type F tumors [papillary adenocarcinoma with compressive and destructive growth]). Tumor subtypes were determined based on the classification of Noguchi *et al.* (3). AAH lesions were included in the current study because these tumors are classified as precancer lesion in World Health Organization classification of lung neoplasms (9). Taking prognosis into consideration, the 96 lesions were classified into four groups; group 1 (lesions of AAH and type A tumor); group 2 (type B tumors); group 3 (type C tumors); group 4 (types D, E, and F tumors).

F18-FDG PET-CT

Patients were asked to fast for 6 h and then subsequently received 3.7 MBq/kg of FDG intravenously followed by PET-CT after 1 h for rest. Combined PET-CT imaging was conducted by using two PET-CT units, Biograph duo (Siemens, Erlangen, Germany) with two rows of detectors, and Gemini (Philips Medical Systems, Best, The Netherlands) with 16 rows of detectors. CT images by Biograph duo were acquired with X-ray tube voltage of 130kV, X-ray tube current of 75mAs, collimations of 2 $\times$ 4 mm, a helical pitch of 3.4, field of views of 50 cm, scan time of 170 s, and exposure time of 0.8 s per rotation. CT images by the Gemini unit were acquired with tube X-ray voltage of 120kV, X-ray tube current of 150 mAs, collimations of 8 $\times$ 3 mm, a helical pitch of 7, field of views of 60 cm, scan time of 120 s, and exposure time of 1 s per rotation. PET images of both PET-CT units, encompassing the same field of view as the CT images, were acquired in 120–170 s per bed position. Both CT and PET scans were obtained from the vertex to the femur under free-breathing.

PET-CT images were retrospectively evaluated visually and semi-quantitatively by two experienced radiologists (TH and SW) without knowledge of the patient's data. By visual assessment, when the accumulation of the tracer in the lesions was greater than that of the surrounding normal lung, the lesions were diagnosed as positive. In doubtful cases the final diagnosis was made by consensus of both radiologists. Semi-quantitative analyses were made by averaged values of SUV_{max} of lesions measured by both radiologists using the following formula (10):

$$SUV_{max} = \frac{\text{Counts.CF [kBq/ml/kg]}}{\text{ID [kBq/ml]/mass [kg]}} \times \text{Decay factor}$$

where CF indicates calibration factor and ID injected dose. The SUV_{max} was obtained by selecting volumetric regions of interest within the pulmonary nodule to include all tumor tissue but not any non-tumor tissue with potentially higher SUV_{max} than that of the tumor. Attenuation-corrected PET images were used for the calculation.

Statistical analyses

As the prognosis of patients worsens with the progression of the number of group categories, proportions of positive PET-CT diagnoses and mean SUV_{max} of lesions of the four groups were analyzed using trend tests to examine if there was a linear correlation between the proportions of positive PET-CT diagnoses or mean PET SUV_{max} and the progression of the number of group categories. Cochran-Armitage test was used for the assessment of the proportions and Jonckheere-Terpstra test for the assessment of mean values. The Mann-Whitney U test was used to compare difference in the mean SUV_{max} of each pair of the four groups and the Fisher's exact test was used to compare the proportions of positive PET-CT diagnoses of each pair of the four group categories. Then, an optimal threshold of SUV_{max} was proposed to best discriminate groups 3 or 4 (patients with poor prognosis) from groups 1 or 2 (patients with good prognosis).

Furthermore, the false-negative rates of the optimal threshold for predicting tumors of poor prognosis between the nodules of <1 cm and $\geq$1 cm were compared to examine the effect of nodule size on SUV_{max}. Similarly, we also compared the false-negative rates of the criterion between the nodules in the basal lung segments and in the other segments to evaluate the effect of respiratory motion on SUV_{max}. A P value <0.05 was considered to

Table 1 The relation between proportions of positive PET-CT or mean SUV_{max} of lesions and histologic grading

	Group 1 (AAH, Type A) ($n = 10$)	Group 2 (Type B) ($n = 12$)	Group 3 (Type C) ($n = 42$)	Group 4 (Types D, E, F) ($n = 32$)	*P* value
Positive PET-CT findings (%)	20* (2/10)	58*† (7/12)	90† (38/42)	91 (29/32)	<0.05
SUV_{max} (mean ± SD)	0.57 ± 0.23	0.90 ± 0.45‡	2.38 ± 1.94‡	3.47 ± 2.68	<0.05

*$P = 0.04$ between groups 1 and 2
†$P = 0.02$ between groups 2 and 3
‡$P < 0.01$ between groups 2 and 3
Group 1, atypical adenomatous hyperplasia and type A tumors; group 2, type B tumors; group 3, type C tumors; group 4, type D, E, and F tumors

indicate a statistically significant difference. All of the statistical calculations were performed using SPSS software (SPSS Inc., Chicago, IL, USA).

Results

Group 1 included 10 lesions, group 2 12, group 3 42, and group 4 32. The size of the nodules ranged from 5 to 20 mm. Of the 96 lesions, nine lesions measured < 1 cm and 17 of the lesions were located in the basal segments of the lung. As shown in Table 1, a statistically significant linear trend was seen in the proportions of positive PET-CT diagnoses. According to the advancement from group 1 through group 2 to group 3, and then to group 4, the proportions of positive PET-CT diagnoses significantly increased ($P < 0.05$). The proportions of positive PET-CT diagnoses in group 3 were significantly greater than in group 2 ($P = 0.02$), which again was significantly greater than that in group 1 ($P = 0.04$). Similarly, there was a statistically significant linear trend in the mean SUV_{max} of the four groups. According to the advancement from group 1 through group 2 to group 3, and then to group 4, the mean SUV_{max} of lesions significantly increased ($P < 0.05$). The mean SUV_{max} in group 3 was significantly greater than that in group 2 ($P < 0.01$).

Using the SUV_{max} for predicting patients with poor prognosis (group 3 or group 4), a threshold of 0.42 showed the highest accuracy of 84% with 95% sensitivity, 50% specificity, 86% positive predictive value, and 73% negative predictive value. With use of this optimal criterion for predicting patients with poor prognosis, there were 70 true-positive diagnoses (Fig. 1), 11 false-positive diagnoses (Fig. 2), 11 true-negative diagnoses (Fig. 3), and four false-negative diagnoses (Fig. 4). When a threshold of 2.05 was used for predicting patients with poor prognosis, no false-positive cases were included (100% specificity). However, this threshold showed poor sensitivity (49%) with 100% positive predictive value and 36% negative predictive value. Visual assessment showed similar accuracy of 83% with 90% sensitivity, 59% specificity, 88% positive predictive value, and 65% negative predictive value.

No significant differences were seen in the false-negative rates between the lesions of <1 cm (0%, 0/3 nodules) and ≥1 cm (5.6%, 4/71 nodules) or between the lesions in basal segments (6.7%, 1/15 nodules) and in the other segments of the lung (5.1%, 3/59 nodules).

Discussion

In the current study, as the histology grading of pulmonary tumors advanced, both SUV_{max} and proportions of positive diagnoses on PET-CT statistically significantly increased. When the optimal threshold of 0.42 for SUV_{max} was used, 84% accuracy for predicting tumors of poor prognosis (types C-F tumors) was obtained. Visual diagnoses showed similar accuracy of 83%. These results may indicate that the tumor aggressiveness may increase as the histologic grade progresses from type A tumors through type B tumors to type C tumors and then to types D, E, and F tumors.

Maeda *et al.* (7) analyzed the relationship between PET-CT and tumor subtypes of 54 patients defined by Noguchi *et al.* (3). They divided those tumors into two groups, one with good prognosis (type A and type B tumors) and the other with poor prognosis (types C-F tumors) and concluded that an optimal threshold of 1.0 for SUV_{max} yielded 93% accuracy for prediction of patients

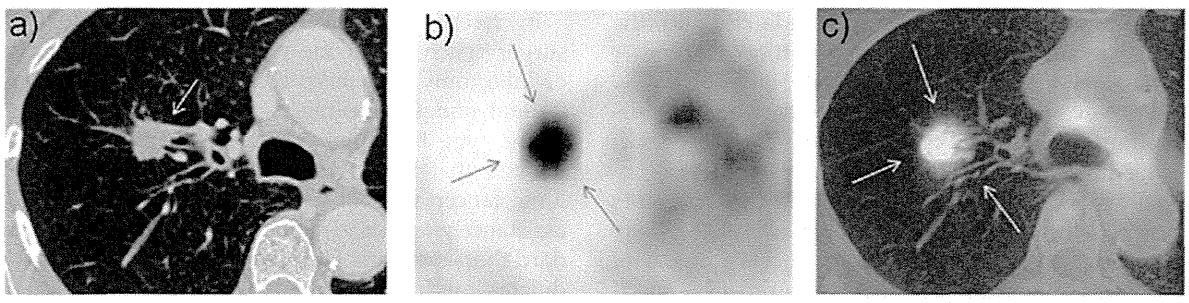

Fig. 1 True-positive diagnoses in a 76-year-old woman with group 4 (type D tumor). (a) Thin-section CT shows a spiculated solid nodule (arrow). Transverse PET image (b) and a fusion image of PET-CT (c) show a strong accumulation in the nodule (a SUV_{max} of 9.7; arrows). Visual assessment was positive. The SUV_{max} of lesion exceeded an optimal threshold of 0.42 and therefore, correct diagnoses of tumor of poor prognosis was made

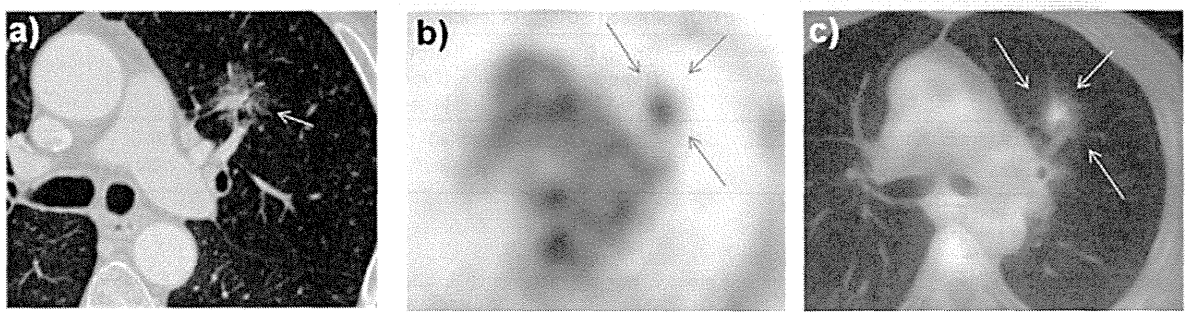

Fig. 2 False-positive diagnoses in a 70-year-old man with group 2 (type B tumor). (a) Thin-section CT shows a spiculated mixed ground-glass opacity nodule (arrow). Transverse PET image (b) and a fusion image of PET-CT (c) show an increased accumulation in the nodule (a SUV_{max} of 2.0; arrows). Visual assessment was positive. The SUV_{max} of lesion exceeded an optimal threshold of 0.42 and therefore, the patient was incorrectly diagnosed as having tumor of poor prognosis

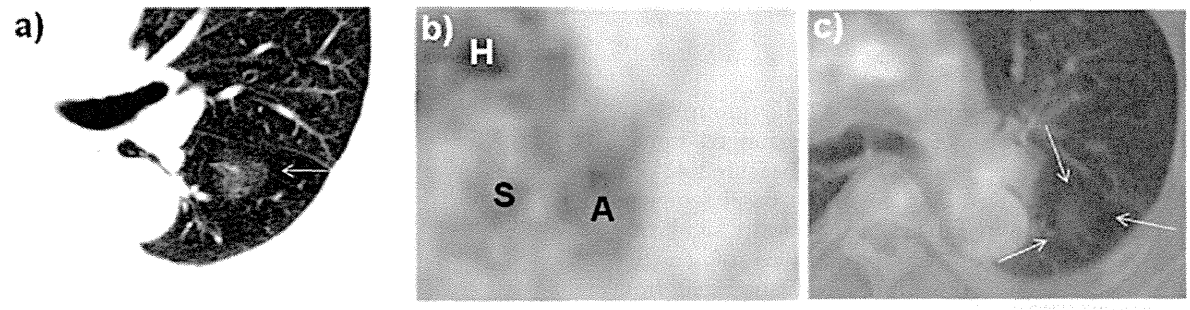

Fig. 3 True-negative diagnoses in a 72-year-old man with group 1 (type A tumor). (a) Thin-section CT shows a ground-glass opacity nodule (arrow). Transverse PET image (b) and a fusion image of PET-CT (c) show no increased accumulation in the nodule (arrows). Visual assessment was negative. The SUV_{max} of lesion measured in the corresponding site of (a) was 0.40, which was smaller than the optimal threshold of 0.42. Therefore, correct diagnoses of good prognosis was obtained. A, descending aorta; H, heart; S, spine

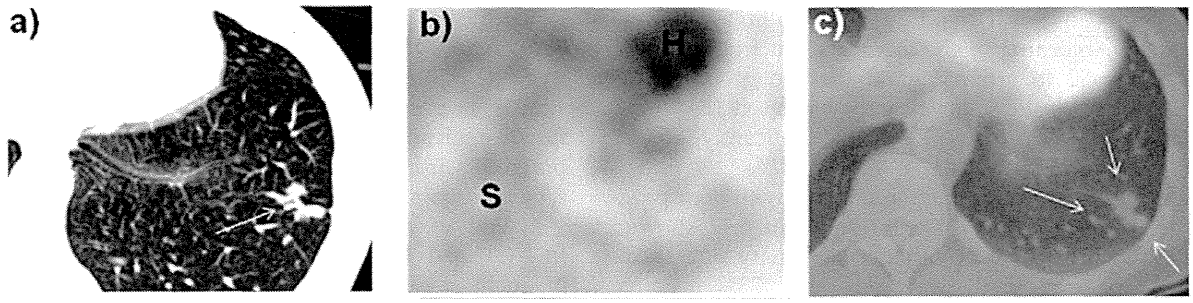

Fig. 4 False-negative diagnoses in a 59-year-old woman with group 3 (type C tumor). (a) Thin-section CT shows a lobulated solid nodule (arrow). Transverse PET image (b) and a fusion image of PET-CT (c) show no increased accumulation in the nodule (arrows). Visual assessment was negative. The SUV_{max} of lesion measured in the corresponding site of (a) was 0.41, which was smaller than the optimal threshold of 0.42. Therefore, this patient was incorrectly diagnosed as having tumor of good prognosis. H, heart; S, spine

with poor prognosis. In the study of Maeda *et al.* (7), the number of patients, especially the proportion of type A tumor, was small and the diagnostic capability of SUV_{max} <1.0 was not evaluated. The correlation between the histology grading of tumor subtypes and visual diagnoses of PET-CT was not assessed either.

In the study of visual interpretation on PET in 37 tumors of Noguchi classification made by Tsunezuka *et al.* (8), diagnostic accuracy for predicting poor prognosis (tumors of types C–F) was 70% with 64% sensitivity and 89% specificity. However, the patients' number was too small to make a statistical analysis and the role of SUV_{max} in those tumors was not studied.

In recent years, it has been suggested that limited surgery such as a wide wedge resection, segmentectomy, or lobectomy with hilar lymph node dissection and mediastinal nodes sampling is feasible for patients with type A and type B tumors (11, 12). Yamamoto *et al.* (13) documented that 5-year survival of patients at early stage of lung cancer who underwent limited surgery with video assistance was comparable to that of patients who had standard thoracotomies. However, preoperative selection of candidates for limited surgery is a serious clinical problem. Thin-section CT analyses succeeded in this selection of patients to some extent (5, 6). Takashima *et al.* (5) evaluated various thin-section CT findings with use of multivariate

analyses for discriminating type C tumors from type A or B tumors and suggested that percentages of ground-glass opacity areas of lesion were useful for discrimination between those two tumor categories. The accuracy (85%) in this study in differentiating type C tumors from type A or B tumors on thin-section CT was comparable to our study of FDG-PET CT.

Regarding the nodal staging of non-small cell lung cancer, it has been reported that FDG-PET is more accurate than CT alone (14, 15). Meta-analysis has demonstrated that FDG-PET was statistically significantly more accurate than spiral CT for identifying lymph node involvement (median sensitivity and specificity 61% and 79%, respectively, for CT and 85% and 90%, respectively, for FDG-PET).

In a comparable study of FDG-PET CT and CT alone, Shim *et al.*, reported that FDG-PET CT was more accurate (79% for CT alone and 86% for FDG-PET CT) and more specific (69% for CT alone and 84% for FDG-PET CT) than CT alone for staging of nodal status of cases of non-small cell lung cancer (15).

No case of type A or B tumors had lymph node metastases and excellent prognosis, while 28% of cases of type C tumors had nodal metastases with poor prognosis (3). There seems to be general agreement that FDG-PET CT is more accurate and more specific than CT for nodal staging of cases of non-small cell lung cancer. The information on nodal status with FDG-PET CT may improve the accuracy in separating tumors with good prognosis from those with poor prognosis and may enhance the confidence of surgeons in selecting appropriate surgical methods. When a pulmonary nodule with SUV_{max} $\leq$0.42 or with visually negative result on FDG-PET CT shows no evidence of nodal metastases on FDG-PET CT, a highly likely diagnosis will be a type A or B tumor rather than type C tumor and limited surgery may be indicated. Standard thoracotomy with nodal dissection may be needed for a pulmonary nodule of SUV_{max} $\geq$2.05 regardless of presence or absence of nodal metastases on FDG-PET CT, because SUV_{max} $\geq$2.05 invariably indicated type C tumors in our series.

In the recently published literature on a new classification of lung adenocarcinoma, type A and B tumors were classified as adenocarcinoma *in situ*, whereas type C tumors were classified into two categories, one being minimally invasive adenocarcinoma and the other lepidic predominant adenocarcinoma; the former one has small foci of invasion with excellent prognosis similar to adenocarcinoma *in situ* and the latter one indicates invasive adenocarcinoma with poor prognosis (16, 17).

In this study, two different PET/CT scanners were used. Although a little difference in SUV_{max} of the two scanners was unavoidable, we tried to minimize the difference by using phantom adjustment at regular time-intervals. Small lesions are reported to show artifactually low SUV_{max} from partial volume effects and SUV_{max} of pulmonary nodules located near the diaphragm have a risk of being underestimated from respiratory motion (18, 19). However, in our series such phenomena were not observed.

In conclusion, FDG-PET CT may be beneficial for discrimination of tumor subtypes and therefore, may contribute to not only selection of candidates for limited surgery but also prediction of prognosis of patients with peripheral T1a adenocarcinoma of the lung.

ACKNOWLEDGEMENTS

We thank Takahashi Horinouchi for providing radiological data.

Conflict of interest: None.

REFERENCES

1 Jemal A, Siegel R, Xu J, *et al.* Cancer statistics, 2010. *CA-Cancer J Clin* 2010;**60**:277–300
2 Travis WD, Travis LB, Devesa SS. Lung cancer. *Cancer* 1995;**75**:191–202
3 Noguchi M, Morikawa A, Kawasaki M, *et al.* Small adenocarcinoma of the lung. *Cancer* 1995;**75**:2844–52
4 Schneider BJ. Non-small cell lung cancer staging: proposed revisions to the TNM system. *Cancer Imaging* 2008;**8**:181–5
5 Takashima S, Li F, Maruyama Y, *et al.* Discrimination of subtypes of small adenocarcinoma in the lung with thin-section CT. *Lung Cancer* 2002;**36**:175–82
6 Kodama K, Higashiyama M, Yokouchi H, *et al.* Prognostic value of ground-glass opacity found in small lung adenocarcinoma on high-resolution CT scanning. *Lung Cancer* 2001;**33**:17–25
7 Maeda R, Isowa N, Onuma H, *et al.* The maximum standardized uptake values on positron emission tomography to predict the Noguchi classification and invasiveness in clinical stage IA adenocarcinoma measuring 2 cm or less in size. *Interact Cardiovasc Thorac Surg* 2009;**9**:70–3
8 Tsunezuka Y, Shimizu Y, Tanaka N, *et al.* Positron emission tomography in relation to Noguchi's classification for diagnoses of peripheral non-small-cell lung cancer 2 cm or less in size. *World J Surg* 2007;**31**:314–7
9 Brambilla E, Travis WD, Colby TV, *et al.* The new World Health Organization classification of lung tumours. *Eur Respir J* 2001;**18**:1059–68
10 Agarwal M, Brahmanday G, Bajaj SK, *et al.* Revisiting the prognostic value of preoperative ^{18}F-fluoro-2-deoxyglucose (^{18}F-FDG) positron emission tomography (PET) in early-stage (I & II) non-small cell lung cancers (NSCLC). *Eur J Nucl Med Mol Imaging* 2009;**37**:691–8
11 Ohde Y, Nagai K, Yoshida J, *et al.* The proportion of consolidation to ground-glass opacity on high resolution CT is a good predictor for distinguishing the population of noninvasive peripheral adenocarcinoma. *Lung Cancer* 2003;**42**:303–10
12 Matsuguma H, Yokoi K, Anraku M, *et al.* Proportion of ground-glass opacity on high-resolution computed tomography in clinical T1N0M0 adenocarcinoma of the lung: A predictor of lymph node metastasis. *J Thorac Cardiovasc Surg* 2002;**124**:278–84
13 Yamamoto K, Ohsumi A, Kojima F, *et al.* Long-term survival after video-assisted thoracic surgery lobectomy for primary lung cancer. *Ann Thorac Surg* 2010;**89**:353–9
14 Gould MK, Kuschner WG, Rydzak CE, *et al.* Test performance of positron emission tomography and computed tomography for mediastinal staging in patients with non-small-cell lung cancer: a meta-analysis. *Ann Intern Med* 2003;**139**:879–92
15 Shim SS, Lee KS, Kim BT, *et al.* Non-small cell lung cancer: prospective comparison of integrated FDG PET/CT and CT alone for preoperative staging. *Radiology* 2005;**236**:1011–9
16 Borczuk AC, Qian F, Kazeros A, *et al.* Invasive size is an independent predictor of survival in pulmonary adenocarcinoma. *Am J Surg Pathol* 2009;**33**:462–9
17 Travis WD, Brambilla E, Noguchi M, *et al.* IASLC/ATS/ERS International multidisciplinary classification of lung adenocarcinoma. *J Thorac Oncol* 2011;**6**:244–85
18 Soret M, Bacharach SL, Buvat I. Partial-volume effect in PET tumor imaging. *J Nucl Med* 2007;**48**:932–45
19 Wenner MK, Parker JA, Kolodny GM, *et al.* Respiratory gating enhances imaging of pulmonary nodules and measurement of tracer uptake in FDG PET/CT. *Am J Roentgenol* 2009;**193**:1640–5

European Journal of Radiology 82 (2013) e623–e627

Contents lists available at ScienceDirect

European Journal of Radiology

journal homepage: www.elsevier.com/locate/ejrad

Adenocarcinoma of the lung with scattered consolidation: Radiological–pathological correlation and prognosis

Binghu Jiang[a,b,*], Shodayu Takashima[b], Tomoaki Hakucho[b], Numasaki Hodaka[b], Tomita Yasuhiko[c], Higashiyama Masahiko[c]

[a] Thoracic Medical Center and Department of Radiology, BenQ Hospital, Nanjing Medical University, 71 Hexi Street, Nanjing, Jiangsu 210019, China
[b] Department of Diagnostic Radiological Imaging, Division of Allied Health Sciences, Osaka University Graduate School of Medicine, 1-7 Yamadaoka, Suita, Osaka 565-0871, Japan
[c] Osaka Medical Center for Cancer and Cardiovascular Diseases, 1-3-3 Nakamichi, Higashinari-ku, Osaka 537-0025, Japan

ARTICLE INFO

Article history:
Received 1 April 2013
Received in revised form 4 June 2013
Accepted 13 June 2013

Keywords:
Scattered consolidation
Adenocarcinoma
Lung
Prognosis

ABSTRACT

Purpose: To investigate the clinicopathological features and prognosis in patients with adenocarcinoma of the lung with scattered consolidation (ALSC).
Materials and methods: Between January 2006 and March 2010, 139 consecutive patients with lung adenocarcinoma of ≤3 cm, who underwent pulmonary resection for lung cancer, were investigated retrospectively. Radiologic classification was based on the findings of thin-section CT such as the presence of consolidation or ground-glass opacity (GGO). Type I ($n=15$) and Type II ($n=14$), showed a pure GGO and a mixed GGO with consolidation <50%, respectively. Type IV ($n=38$) and Type V ($n=52$) showed a mixed GGO with consolidation ≥50% and a pure consolidation, respectively. Type III ($n=20$) was the adenocarcinoma of the lung with scattered consolidation (ALSC). The clinicopathological features and prognosis of ALSC was investigated with comparative analysis and survival analysis.
Results: Because of the similar recurrence rate for Type I and Type II ($P=1.000$), Type IV and Type V ($P=0.343$), we merged Type I and Type II as Type I+II, Type IV and Type V as Type IV+V, respectively. In the 20 (14.4%) patients with ALSC, lymph node metastasis was not observed, and it was rare in lymphatic invasion and vascular invasion. On the basis of IASLC/ATS/ERS 2011 classification, 80% of the ALSC were preinvasive lesions. In Noguchi classification, there was no significant difference between Type I+II and ALSC ($P=0.260$). The prognosis of ALSC was similar to Type I+II ($P=0.408$), but better than Type IV+V ($P=0.040$).
Conclusion: Adenocarcinoma of the lung with scattered consolidation (ALSC) on thin-section CT was a relatively favorable prognostic factor.

1. Introduction

Adenocarcinoma of the lung, accounting for 38.5% of all lung cancer [1], has become the most common histologic type largely due to an increase in detection of small and faint nodules on chest radiography, such as ground-glass opacity (GGO) [2]. The proportion of GGO on thin-section CT has been documented to be a significant prognostic factor in adenocarcinoma of the lung [3–7]. However, it is often difficult to measure the proportion of GGO, and there is no generally accepted method for measuring GGO, especially for adenocarcinoma of the lung with scattered consolidation (ALSC) [8]. As a result, there is considerable disagreement among physicians on the diagnosis.

Suzuki et al. [6,8] proposed a radiologic classification of peripheral adenocarcinoma of the lung to aid in determining the optimal management, in which ALSC was considered as a new radiological entity. This new category could be useful for the preoperative evaluation of lung cancer. However, the pathology and prognosis of ALSC has not been documented in detail.

Therefore, we investigated the clinicopathologic features and prognosis of adenocarcinoma of the lung with scattered consolidation (ALSC) in the current study.

2. Materials and methods

This retrospective study was approved by our institutional review board.

* Corresponding author at: Department of Diagnostic Radiological Imaging, Division of Allied Health Sciences, Osaka University Graduate School of Medicine, 1-7 Yamadaoka, Suita, Osaka 565-0871, Japan. Tel.: +81 06 6879 2564; fax: +81 06 6879 2564.
E-mail address: mbhh@live.cn (B. Jiang).

0720-048X/$ – see front matter © 2013 Elsevier Ireland Ltd. All rights reserved.
http://dx.doi.org/10.1016/j.ejrad.2013.06.010

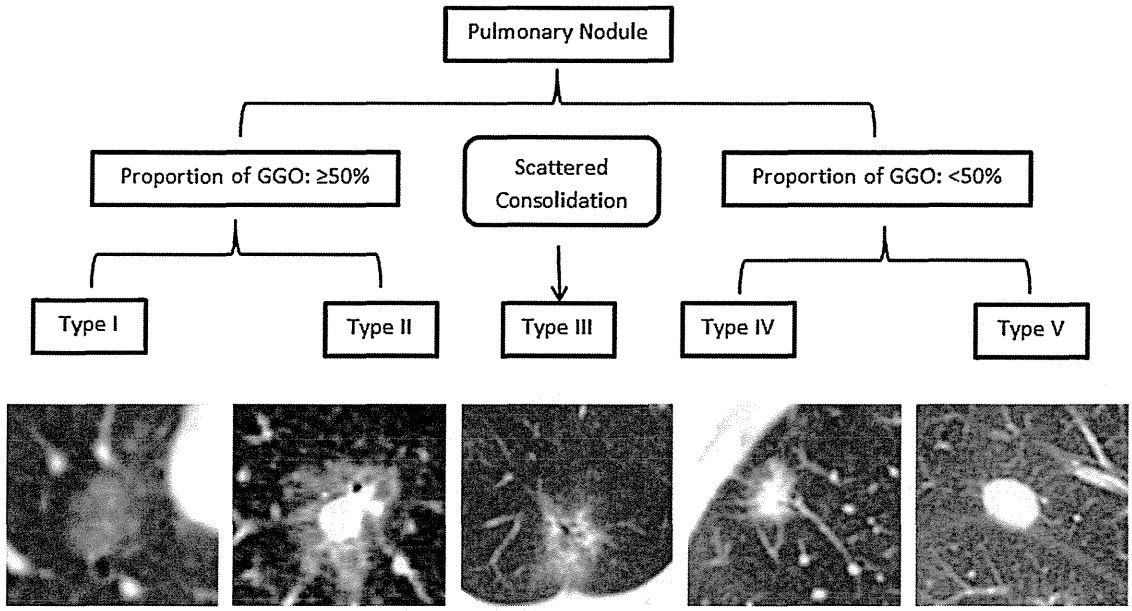

Fig. 1. Flow chart for the radiological classification of adenocarcinoma of the lung and the diagram of Type I–V tumors. Type I tumor is homogeneous in density, and lack of a consolidation component. Type II tumor is heterogeneous in density, and the consolidation component comprises less than 50%. Type III tumor is heterogeneous in density, and the distribution of consolidation is scattered regardless of the extent of consolidation (Fig. 2). Type IV tumor is heterogeneous in density, and the consolidation component comprises 50% or more. Type V tumor is homogeneous in density, and lack of a GGO component.

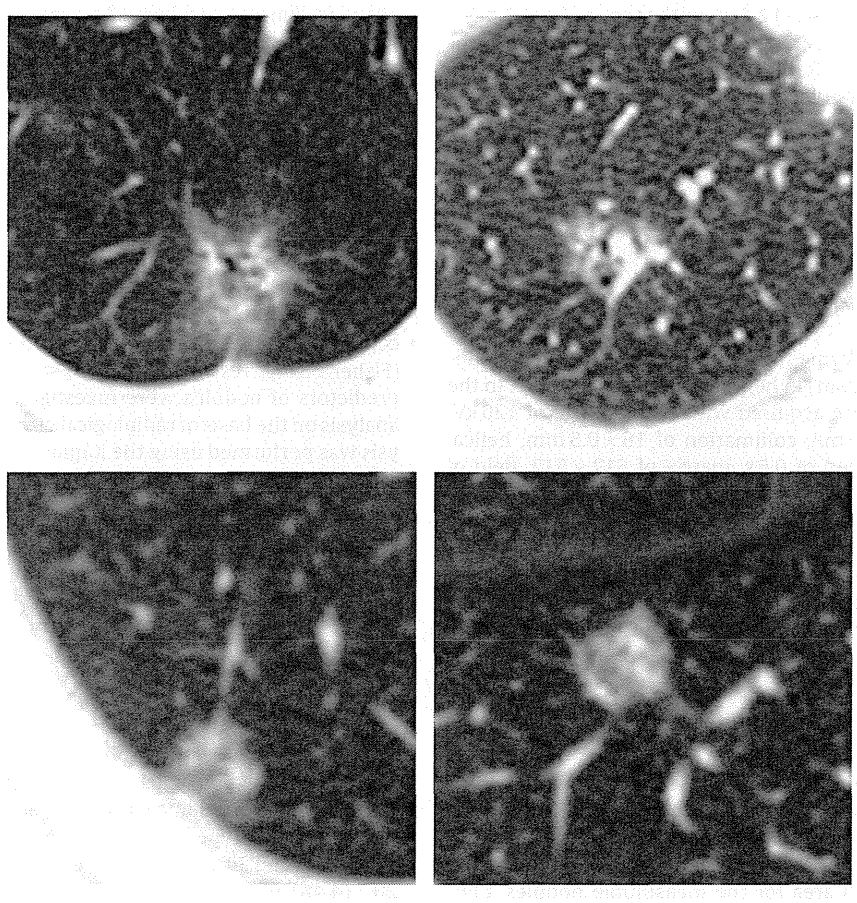

Fig. 2. Type III tumor is heterogeneous in density, and the proportion of consolidation or GGO is difficult to be measured because of their scattered distribution.

Table 1
Radiological classification and clinicopathological features in adenocarcinoma of the lung.

	Type I	Type II	Type III	Type IV	Type V	P[a]
Cases (n)	15	14	20	38	52	-
Mean age (year)	59.7 ± 10.3	61.5 ± 8.9	61.7 ± 9.4	65.0 ± 11.2	65.2 ± 7.6	0.169
Sex (men/women)	10/5	8/6	13/7	24/14	19/33	0.066
Mean size (cm)	1.5 ± 0.8	1.5 ± 0.7	1.8 ± 0.6	1.7 ± 0.7	1.6 ± 0.8	0.100
Lymph node metastasis	1	1	0	2	10	0.081
Lymphatic invasion	0	1	4	13	28	<0.001
Vascular invasion	0	0	0	4	16	0.001
Pleural invasion	1	0	1	2	15	0.003
Noguchi classification						<0.001
A Type	10	4	1	0	0	
B Type	5	6	5	2	0	
C Type	0	4	11	31	25	
D Type	0	0	0	3	7	
E Type	0	0	1	0	10	
F Type	0	0	2	2	10	
IASLC/ATS/ERS 2011[b]						<0.001
AAH + AIS	14	9	6	2	0	
MIA	0	3	10	23	14	
Invasive ade.	1	2	4	13	38	
Recurrence	0	0	1	8	16	<0.001

[a] Kruskal–Wallis Test.
[b] AAH = atypical adenomatous hyperplasia. AIS = adenocarcinoma in situ. MIA = minimally invasive adenocarcinoma. Invasive ade. = invasive adenocarcinoma.

2.1. Patients

Between January 2006 and March 2010, 952 consecutive patients underwent pulmonary resection for lung cancer. Of them, 139 patients (74 men and 65 women; age: 62.8 ± 10.5 years) had solitary primary adenocarcinoma of 3 cm or less in size and underwent preoperative thin-section CT scans. The interval of thin-section CT and surgery was 14 ± 12 days with range of 1 to 33 days. Limited resection (wedge resection or segmentectomy) (n = 29) or lobectomy (n = 110) was performed for surgery. The length of survival was defined as the interval in days between the date of surgical resection of tumor and the date of either recurrence or the last follow-up.

The sections of specimens were stained with hematoxylin–eosin and Elastica van Gieson. All slides were reviewed by a pathologist (T.Y., with 20-year experience in surgical pathology).

2.2. Thin-section CT technology

All CT scans were performed with a 16-slice CT scanner (Aquilion 16, Toshiba, Tokyo, Japan) in helical mode from the apex to the lung base. CT images were acquired with tube voltage of 120 kV, tube current of 240–300 mA, collimation of 16 × 0.5 mm, helical pitch of 1.0, rotation speed of 0.5 s, matrix of 512 × 512, field of view (FOV) of 32.0 cm, reconstruction thickness of 1.0 mm, and bone reconstruction algorithm. Without knowledge of pathology and prognosis, two observers (B.J. and S.T., with 5-year and 30-year experience in chest radiology, respectively) independently evaluated the images with a monitor (AZE VirtualPlace™) (window level = −600 HU, window width = 1200 HU). The final findings were determined by consensus and averaged values of measurements.

2.3. Radiologic criteria for grouping

The radiological findings were assessed in terms of nodule size (the greatest transverse diameter) and status of GGO component. GGO was defined as hazy increased opacity of lung, with preservation of bronchial and vascular margins. The proportion of GGO was calculated with area for the measurable nodules. Consolidation was defined as a homogeneous increase in pulmonary parenchymal attenuation that obscured the margins of vessels and airway walls [9].

Adenocarcinoma of the lung with scattered consolidation (ALSC) was defined as consolidation whose distribution was scattered and was difficult to be measured on thin-section CT [8]. We divided the 139 adenocarcinomas of the lung into five groups (Type I–Type V) based on the radiologic appearance (Fig. 1). Type I was homogeneous in density, and lack of a consolidation component. Type II was heterogeneous in density, and the consolidation component comprised less than 50%. Type III was heterogeneous in density, and the distribution of consolidation was scattered regardless of the extent of consolidation (Fig. 2). Type IV was heterogeneous in density, and the consolidation component comprised 50% or more. Type V was homogeneous in density, and lack of a GGO component.

2.4. Statistical analysis

A kappa value was used to assess the inter-observer agreement for radiological classification of nodules. To compare the clinicopathological features, Kruskal–Wallis Test and Chi-Square Test (Fisher's Exact Test) were used for statistical analysis. The invasive predictors of nodules were investigated with Logistic regression analysis on the basis of radiological classification. The survival analysis was performed using the Kaplan–Meier method with log-rank test and Cox proportional hazard model. Two-tailed P value of less than 0.05 was considered to be significant. The statistical analysis was performed with SPSS software (PASW Statistics 18; SPSS Inc., Chicago, IL, USA).

3. Results

The kappa value was 1.00 for Type I, 0.91 for Type II, 1.00 for Type III, 0.92 for Type IV, and 1.00 for Type V. The clinicopathological features of the patients were compared based on radiological classification (Table 1). Because the recurrence rate was identical between Type I and Type II (P = 1.000), we merged Type I and Type II as Type I + II. The same situation was seen in Type IV and Type V (P = 0.343), and Type IV and Type V were merged as Type IV + V.

ALSC, Type III adenocarcinoma of the lung, was observed in 20 (14.4%) of 139 patients. There were 13 men and 7 women who ranged in age from 49 to 78 years (mean 61.7 ± 8.1 years).

Table 2
Comparison of clinicopathological features between Type III vs. Type I + II and Type III vs. Type IV + V.

Variable	Type I + II	*P*	Type III	*P*	Type IV + V
Cases (*n*)	29	–	20	–	90
Mean age (year)	60.6 ± 9.2	0.712[b]	61.7 ± 9.4	0.132[b]	65.1 ± 9.8
Sex (men/women)	18/11	1.000[a]	13/7	0.218[a]	43/47
Mean size (cm)	1.5 ± 0.8	0.001[b]	1.8 ± 0.6	0.271[b]	1.7 ± 0.8
Lymph node metastasis	2	0.507[a]	0	0.119[a]	12
Lymphatic invasion	1	0.144[a]	4	0.044[a]	41
Vascular invasion	0	–	0	0.021[a]	20
Pleural invasion	1	1.000[a]	1	0.186[a]	17
Noguchi classification		0.260[a]		0.018[a]	
A Type	14		2		0
B Type	11		10		2
C Type	4		6		56
D Type	0		0		10
E Type	0		1		10
F Type	0		1		12
IASLC/ATS/ERS 2011[b]		0.002		<0.001	
AAH + AIS	23		6		2
MIA	3		10		37
Invasive ade.	3		4		51
Recurrence	0	0.408[a]	1	0.040[a]	24

[a] Chi-Square Test (Fisher's Exact Test).
[b] Independent samples *t* test.

Compared with Type I + II, the ALSC was significantly bigger in the maximum diameter ($P = 0.001$) and was more invasive based on IASLC/ATS/ERS 2011 criterion ($P = 0.002$). Compared with Type IV + V, the ALSC was lack of lymphatic invasion, vascular invasion and recurrence, and was less invasive based on Noguchi ($P = 0.018$) and IASLC/ATS/ERS 2011 criterion ($P < 0.001$) (Table 2). The Logistic regression analysis showed that the ALSC (Type III) was a favorable predictor for lymphatic invasion with a relative risk of 0.299 [95% confidence interval (CI): 0.093, 0.964] ($P = 0.043$), along with Type I + II with a relative risk of 0.043 [95% CI: 0.006, 0.327] ($P = 0.002$).

Mean time (days) of follow-up was 1735 ± 646 (S.D.) and 25 patients showed tumor recurrence after surgery, which was seen in the lung ($n = 5$), lymph node ($n = 14$), brain ($n = 3$), kidney ($n = 2$), and bone ($n = 1$). Of the 25 carcinomas with recurrence, one was in Type III (ALSC) and 24 were in Type IV + V. The operative procedure (limited resection or lobectomy) had no effect on prognosis ($P = 0.786$) (Table 3). The Kaplan–Meier analysis showed the prognosis of Type I + II ($P = 0.003$) or Type III ($P = 0.042$) was better than Type IV + V (Fig. 3), and there was no significant difference between Type I + II and Type III ($P = 0.229$). Cox proportional hazard model showed the odds ratio of Type III to Type IV + V was 0.159 with 95% CI of 0.022 to 0.897 ($P = 0.047$) on the risk of recurrence, indicating ALSC was a protective or favorable factor. The 5-year disease-free survival rate was 100%, 95%, and 73.3% in patients with lung adenocarcinoma of Type I + II, Type III, and Type IV + V, respectively.

Table 3
The effect of operative procedure on prognosis of lung cancer.

	Limited resection	Lobectomy	*P* value[a]
Nodule Type			<0.001
Type I	10	5	
Type II	8	6	
Type III	4	16	
Type IV	5	33	
Type V	2	50	
Recurrence			0.786
Yes	6	19	
No	23	91	

[a] Chi-Square Test.

4. Discussion

In the current study, adenocarcinoma of the lung with scattered consolidation (ALSC), as a new radiological entity for lung adenocarcinoma, was documented to have a similar prognosis with adenocarcinoma manifesting as pure GGO or mixed GGO with consolidation of <50%, which has been confirmed as a favorable adenocarcinoma of the lung [3–5].

Although there was a statistically significance in size between Type III (1.8 ± 0.6 cm) and Type I + II (1.5 ± 0.8 cm), this difference was lack of clinical significance. Because there was obvious overlap in size between Type III and Type I + II. In recurrence rate between Type III and Type I + II, there was no

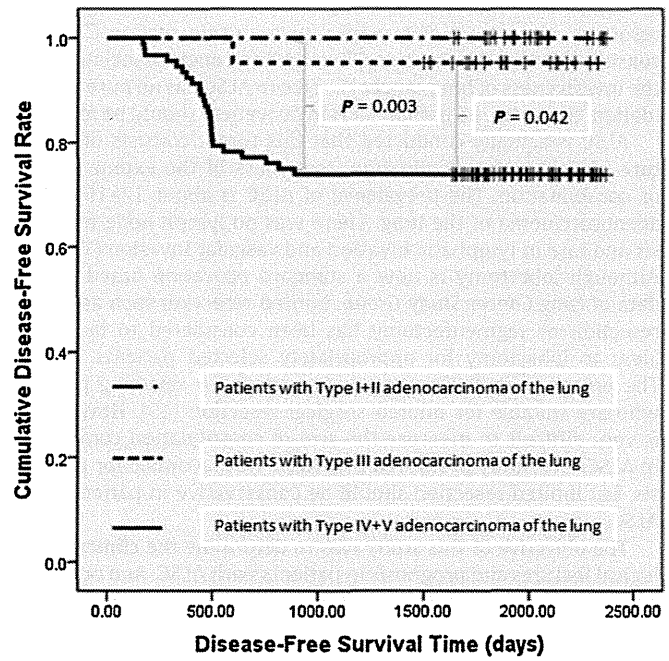

Fig. 3. The disease-free survival curve for patients with Type I + II, Type III and Type IV + V tumor.

Table 4
Review on clinicopathological features of lung cancer with scattered consolidation.

	Suzuki et al. [6]	Matsunaga et al. [8]	Jiang et al.
Case (*n* (%))[a]	43 (12.3%)	71 (12.0%)	20 (14.4%)
Mean age (year)	62.3	66	61.7
Sex (men/women)	19/24	29/42	13/7
Nodule size (cm)			
Range	0.9–2.0	–	1.2–2.8
Mean	1.4	–	1.8
Histology	Adenocarcinoma	Adenocarcinoma	Adenocarcinoma
Lymph node metastasis	0	0	0
Lymphatic invasion	0	12	4
Vascular invasion	1	5	0

[a] The case number of Type III nodules and percentage in all pulmonary nodules.

significant difference. On the basis of IASLC/ATS/ERS 2011 classification, however, more advanced grade was seen in Type III, indicating more invasive than Type I+II. On the other hand, compared with Type IV+V, Type III showed much rare in lymphatic invasion and vascular invasion, and more favorable grade in Noguchi and IASLC/ATS/ERS 2011 classification. In a word, ALSC was a relatively favorable predictor.

A similar radiological finding with ALSC has been reported by Suzuki et al. [6,8]. They reported that ALSC was radiological early adenocarcinoma of the lung, and their pathological features were minimally invasive. As a conclusion, limited resection could be enough for ALSC. However, the lack of prognostic analysis of disease-free survival with Kaplan–Meier method limited that conclusion in their studies. Our study showed that, although ALSC was less invasive, the recurrence was still seen in follow-up. Therefore, regardless of the relatively favorable prognosis of ALSC, limited resection should be conservative in patients with ALSC.

Pathologically, central fibrosis of adenocarcinoma of the lung has been documented to be a prognostic factor [2,10–12]. Active fibroblasts in the central fibrosis have been reported to be associated with a poor prognosis [10]. Active fibroblast is a sign of destruction of the basement membrane by cancer cells, which leads to mesenchymal destruction of the lung. This destruction results in the exclusion of air in the lung, which is a phase of consolidation on CT scan. If the invasion or destruction of the mesenchyme of the lung is minimal, air in the lung remains within the lung cancer, resulting in a ground glass appearance on thin-section CT. Thus, consolidation on thin-section CT could be strongly associated with the invasiveness of lung cancer [7]. Due to ALSC has no pure consolidation, therefore, its pathological invasiveness should be minimal.

ALSC is actually conducted that this tumor consists of a mixture of GGO and consolidation, regardless of the extent of GGO or consolidation. The prevalence of ALSC is about 12–15% of all adenocarcinoma of the lung. There was no lymph node metastasis and rare in lymphatic invasion and vascular invasion (Table 4). Although lobectomy is now a standard operation based on the data of *Lung Cancer Study Group*, limited resection such as wedge resection or segmentectomy has been considered to be equivalent to lobectomy for appropriately selected patients [13,14]. The preoperative GGO status is important for selecting patients who are suitable for limited surgical resection [15]. However, it is very difficult to measure the size of consolidation component in ALSC. Our study prompted that ALSC was favorable for prognosis, but limited resection should be conservative in patients with ALSC.

The objective of this study was to determine the clinicopathological features and prognosis in patients with ALSC. And our result confirmed that the prognosis of ALSC was as good as Type I + II adenocarcinoma of the lung. However, ALSC was more invasive than Type I + II on the basis of IASLC/ATS/ERS 2011 criterion. Therefore, it should be conservative to select the patient with ALSC as candidate for limited resection. However, this study was limited in that it was a retrospective design and the number of patients was relatively small, possibly leading to a sampling bias.

In conclusion, we propose from the present data that adenocarcinoma of the lung with scattered consolidation (ALSC) on thin-section CT was a relatively favorable prognostic factor, but limited resection should be conservative in patients with ALSC.

Conflict of interest statement

The authors report no conflicts of interest.

References

[1] SEER cancer statistics review, 1975–2008. Available at: http://seer.cancer.gov/csr/1975_2008/results_merged/sect_15_lung_bronchus.pdf [accessed 30.01.12].
[2] Travis WD, Brambilla E, Noguchi M, et al. International Association for the Study of Lung Cancer/American Thoracic Society/European Respiratory Society: international multidisciplinary classification of lung adenocarcinoma. Journal of Thoracic Oncology 2011;6:244–85.
[3] Aoki T, Tomoda Y, Watanabe H, et al. Peripheral lung adenocarcinoma: correlation of thin-section CT findings with histologic prognostic factors and survival. Radiology 2001;220:803–9.
[4] Takashima S, Maruyama Y, Hasegawa M, et al. CT findings and progression of small peripheral lung neoplasms having a replacement growth pattern. American Journal of Roentgenology 2003;180:817–26.
[5] Ohde Y, Nagai K, Yoshida J, et al. The proportion of consolidation to ground-glass opacity on high resolution CT is a good predictor for distinguishing the population of non-invasive peripheral adenocarcinoma. Lung Cancer 2003;42:303–10.
[6] Suzuki K, Kusumoto M, Watanabe S, et al. Radiologic classification of small adenocarcinoma of the lung: radiologic–pathologic correlation and its prognostic impact. Annals of Thoracic Surgery 2006;81:413–9.
[7] Suzuki K, Koike T, Asakawa T, et al. A prospective radiological study of thin-section computed tomography to predict pathological noninvasiveness in peripheral clinical IA lung cancer (Japan Clinical Oncology Group 0201). Journal of Thoracic Oncology 2011;6:751–6.
[8] Matsunaga T, Suzuki K, Hattori A, et al. Lung cancer with scattered consolidation: detection of new independent radiological category of peripheral lung cancer on thin-section computed tomography. Interactive Cardiovascular and Thoracic Surgery 2013;16:445–9.
[9] Hansell DM, Bankier AA, MacMahon H, et al. Fleischner Society: glossary of terms for thoracic imaging. Radiology 2008;246:697–722.
[10] Shimosato Y, Suzuki A, Hashimoto T, et al. Prognostic implications of fibrotic focus (scar) in small peripheral lung cancers. American Journal of Surgical Pathology 1980;4:365–73.
[11] Noguchi M, Morikawa A, Kawasaki M, et al. Small adenocarcinoma of the lung. Histologic characteristics and prognosis. Cancer 1995;75:2844–52.
[12] Suzuki K, Yokose T, Yoshida J, et al. Prognostic significance of the size of central fibrosis in peripheral adenocarcinoma of the lung. Annals of Thoracic Surgery 2000;69:893–7.
[13] Yoshikawa K, Tsubota N, Kodama K, et al. Prospective study of extended segmentectomy for small lung tumors: the final report. Annals of Thoracic Surgery 2002;73:1055–8.
[14] Ginsberg RJ, Rubinstein LV. Randomized trial of lobectomy versus limited resection for T1 N0 non-small cell lung cancer. Lung Cancer Study Group. Annals of Thoracic Surgery 1995;60:615–22.
[15] Julian R, Yang P, Stephen D, et al. Non-small cell lung cancer: epidemiology, risk factors, treatment, and survivorship. Mayo Clinic Proceedings 2008;83:584–94.

Oncogene (2012), 1–9

www.nature.com/onc

ORIGINAL ARTICLE

Akt kinase-interacting protein1, a novel therapeutic target for lung cancer with *EGFR*-activating and gatekeeper mutations

T Yamada[1], S Takeuchi[1], N Fujita[2], A Nakamura[2], W Wang[1], Q Li[1], M Oda[3], T Mitsudomi[4], Y Yatabe[5], Y Sekido[6], J Yoshida[7], M Higashiyama[8], M Noguchi[9], H Uehara[10], Y Nishioka[11], S Sone[11] and S Yano[1]

Despite initial dramatic response, epidermal growth factor receptor (EGFR) mutant lung cancer patients always acquire resistance to EGFR-tyrosine kinase inhibitors (TKIs). Gatekeeper T790M mutation in *EGFR* is the most prevalent genetic alteration underlying acquired resistance to EGFR-TKI, and *EGFR* mutant lung cancer cells are reported to be addictive to EGFR/Akt signaling even after acquired T790M mutation. Here, we focused on Akt kinase-interacting protein1 (Aki1), a scaffold protein of PI3K (phosphoinositide 3-kinase)/PDK1 (3-phosphoinositide-dependent protein kinase)/Akt that determines receptor signal selectivity for non-mutated *EGFR*, and assessed its role in *EGFR* mutant lung cancer with or without gatekeeper T790M mutation. Cell line-based assays showed that Aki1 constitutively associates with mutant *EGFR* in lung cancer cells with (H1975) or without (PC-9 and HCC827) T790M gatekeeper mutation. Silencing of *Aki1* induced apoptosis of *EGFR* mutant lung cancer cells. Treatment with *Aki1* siRNA dramatically inhibited growth of H1975 cells in a xenograft model. Moreover, silencing of *Aki1* further potentiated growth inhibitory effect of new generation EGFR-TKIs against H1975 cells *in vitro*. Aki1 was frequently expressed in tumor cells of *EGFR* mutant lung cancer patients (53/56 cases), including those with acquired resistance to EGFR-TKI treatment (7/7 cases). Our data suggest that Aki1 may be a critical mediator of survival signaling from mutant *EGFR* to Akt, and may therefore be an ideal target for *EGFR* mutant lung cancer patients, especially those with acquired EGFR-TKI resistance due to *EGFR* T790M gatekeeper mutation.

Oncogene advance online publication, 8 October 2012; doi:10.1038/onc.2012.446

Keywords: Akt kinase-interacting protein1; *EGFR* mutation; novel therapeutic target; lung cancer

INTRODUCTION

Lung cancer with epidermal growth factor receptor (EGFR)-activating mutations, such as exon 19 deletion and exon 21 L858R point mutation, responds to the EGFR-tyrosine kinase inhibitors (EGFR-TKIs) gefitinib and erlotinib.[1] Recent clinical trials demonstrated much longer progression-free survival for EGFR mutant lung cancer patients when treated with gefitinib compared with conventional chemotherapy.[2,3] However, almost without exception, the responders relapse after various times due to acquiring resistance to EGFR-TKIs.[1,4]

The development of gatekeeper mutations, such as T315I in Abl,[5] D473H in SMO[6] and L1196M in ALK,[7] is the most common mechanism of acquired TKI resistance.[8] In cases of *EGFR* mutant lung cancer, *EGFR* T790M mutation is detected in about 50% of patients with acquired resistance to EGFR-TKIs.[4,8,9] T790M mutation results in increased EGFR affinity to adenosine triphosphate, reducing binding of EGFR-TKIs, and thus inducing resistance.[10] However, *EGFR* mutant lung cancer cells with T790M mutation are still dependent on EGFR-mediated signaling,[10] and therefore further elucidation of mutant EGFR-mediated signaling may facilitate the development of novel effective therapeutic strategies against lung cancer with *EGFR* mutations, including T790M gatekeeper mutation.

New generation EGFR-TKIs, such as irreversible EGFR-TKIs and mutant EGFR selective TKIs, were expected to overcome acquired resistance caused by T790M secondary mutation.[11–15] However, several irreversible EGFR-TKIs failed to meet primary end points in clinical trials in EGFR-TKI-refractory lung cancer and induced severe adverse effects, such as diarrhea, skin rush/acne, stomatitis and nail effect.[1,16] More recently, a phase Ib trial of EGFR dual inhibition with irreversible EGFR-TKI afatinib plus anti-EGFR monoclonal antibody cetuximab indicated with a 40% objective response rate in 47 patients with EGFR-TKI acquired resistance,[17] suggesting that many tumors are still addicted to the EGFR signaling pathway, including *EGFR* T790M gatekeeper mutation in clinical trials. Therefore, new intensification treatment targeting EGFR signaling is expected to get for more clinical benefit, whereas the feasibility of these strategies should be evaluated carefully in clinical trials.

Receptor tyrosine kinases, such as EGFR, PDGFRs and VEGFRs, utilize several common downstream signaling pathways, including MAPK/ERK and PI3K/Akt, while each receptor shows different or specific biological activity after ligand stimulation. Scaffold proteins that can simultaneously interact with two or more protein binding partners are thought to ensure specificity as well as temporal regulation of signal transduction. Thus, scaffold

[1]Division of Medical Oncology, Cancer Research Institute, Kanazawa University, Kanazawa, Japan; [2]Cancer Chemotherapy Center, Japanese Foundation for Cancer Research, Tokyo, Japan; [3]Department of General and Cardiothoracic Surgery, Kanazawa University, Kanazawa, Japan; [4]Department of Thoracic Surgery, Aichi Cancer Center Hospital, Nagoya, Japan; [5]Department of Pathology, Aichi Cancer Center Hospital, Nagoya, Japan; [6]Division of Molecular Oncology, Aichi Cancer Center Research Institute, Nagoya, Japan; [7]Department of Thoracic Oncology, National Cancer Center Hospital East, Kashiwa, Japan; [8]Department of Thoracic Surgery, Osaka Medical Center for Cancer and Cardiovascular Diseases, Osaka, Japan; [9]Department of Pathology, Institute of Basic Medical Sciences, University of Tsukuba, Tsukuba, Japan; [10]Department of Molecular and Environmental Pathology, Institute of Health Biosciences, The University of Tokushima Graduate School, Tokushima, Japan and [11]Department of Respiratory Medicine & Rheumatology, Institute of Health Biosciences, The University of Tokushima Graduate School, Tokushima, Japan. Correspondence: Dr T Yamada, Division of Medical Oncology, Cancer Research Institute, Kanazawa University, Takara-machi 13-1, Kanazawa, Ishikawa 920-0934, Japan.
E-mail: tadaakiy@med.kanazawa-u.ac.jp
Received 9 April 2012; revised 7 August 2012; accepted 9 August 2012

proteins may be important targets for regulating receptor-mediated signaling. There is accumulating evidence that Akt signaling is essential for mediating survival signals in *EGFR* mutant lung cancer cells.[18,19] Although several molecules, including KSP,[20] Paxillin,[21] RKIP,[22] and JIP-1,[23] are known to act as scaffolds for MAPK-ERK,[24] scaffold proteins for Akt have not been well documented. Recently, we reported Akt kinase-interacting protein1 (Aki1) as the first identified scaffold in the PI3K/PDK1/Akt pathway. Aki1 selectively forms a complex with EGFR and Akt in response to EGF stimulation, mediates Akt activation by PDK1, and hence contributes to cell survival and proliferation.[25] However, Aki1, the scaffold proteins for therapeutic target in cancers, have yet to be identified.

In the present study, we examined whether Aki1 would act as a determinant of receptor signaling selectivity of mutant EGFR and could be a therapeutic target for *EGFR* mutant lung cancer, including that with T790M gatekeeper mutation.

RESULTS

High levels of Aki1 protein expression in *EGFR* mutant lung cancer cell lines

As the first step to assess the involvement of Aki1 in EGFR-mediating signal of lung cancer cells, we examined the expression of Aki1 protein and its associated proteins (PDK1, Akt and EGFR) in five human lung adenocarcinoma cells with or without *EGFR* mutations, comparing that in two human lung embryonic fibroblast cell lines, by western blotting (Figure 1a). All of the cell lines examined expressed Aki1 and PDK1 protein at various levels. The levels of Aki1 tend to be higher in EGFR mutant lung cancer cell lines than in lung fibroblast cell lines.

EGFR was also detected in all lung cancer and fibroblast cell lines at various levels. Interestingly, phosphorylated EGFR was detected in EGFR mutant lung cancer cell lines, but not detected in EGFR wild-type lung cancer cell lines and fibroblast cell lines. The co-detection of Aki1 and phosphorylated EGFR in these cell lines suggested interactions between Aki1 and mutant EGFR because Aki1 was shown to bind preferentially to activated wild-type EGFR.[25]

Aki1 constitutively associates with *EGFR* without ligand stimulation in *EGFR* mutant lung cancer cells

To determine the role of Aki1 in the EGFR/PDK1/Akt pathway, we examined the association between Aki1 and EGFR by immunoprecipitation. Aki1 constitutively associated with EGFR in all three *EGFR* mutant lung cancer cell lines (Figure 1b). Consistent with the results of previous studies,[25] Aki1 did not associate with IGF-1 R, irrespective of IGF-1 stimulation, indicating selective binding of Aki1 to EGFR (Figure 1b). Moreover, treatment with EGFR-TKI did not affect the association between Aki1 and EGFR/PDK1/Akt (Supplementary Figure S1). These results further suggest that Aki1 may be involved deeply in signal transduction through mutant EGFR.

Specific downregulation of *Aki1* inhibits cell viability and induces cell apoptosis in *EGFR* mutant lung cancer cells

To determine the role of Aki1 in *EGFR* mutant lung cancer cell lines, we used specific small interfering RNA (siRNA) for *Aki1* knockdown. Treatment with *Aki1*-specific siRNA suppressed Aki1 protein expression, and more decreased the viability of *EGFR* mutant cells (PC-9, HCC827 and H1975) than *EGFR* wild-type cells (A549 and PC14PE6) (Figure 2a and Supplementary Figure S2). To confirm the specificity of the *Aki1* siRNA used, we constructed RNA interference (RNAi)-resistant *Aki1* cDNA by mutating the sequence targeted by *Aki1* siRNA without changing the amino acid sequence. Transfection of wild-type *Aki1* or RNAi-resistant *Aki1* resulted in increased expression of Aki1 protein in PC-9 cells (Supplementary Figure S3A). Treatment with *Aki1* siRNA attenuated Aki1 protein expression and cell viability in parental and even in wild-type *Aki1*-transfected cells (Supplementary Figures S3B and C). However, *Aki1* siRNA did not downregulate exogenous Aki1 in RNAi-resistant *Aki1* cDNA-transfected cells. Transfection of RNAi-resistant *Aki1* cDNA overcame the *Aki1* siRNA-mediated decrease in cell viability (Supplementary Figure S3C), indicating the specificity of siRNA to *Aki1*. On the other hand, the effects of *Aki* siRNA in lung fibroblasts, MRC-5 and IMR-90, were only marginal (Figure 2a), suggesting that Aki knockdown selectively inhibits viability of cancer cells with dependent EGFR signal, especially in *EGFR* mutant lung cancer cells. In addition, to rule out any bystander effect of the siRNA, we performed cell culture using two color labeling. We found that *Aki1*-1 siRNA did not show any discernible bystander effect. Therefore, we conclude that the bystander effect is not the primary mechanism by which the *Aki1*-1siRNA treatment inhibited tumor cell growth, under our experimental conditions (Supplementary Figure S5A and B). Therefore, we focused solely on EGFR mutant lung cancer cells. Western blotting analyses indicated that *Aki1* knockdown reduced phosphorylation of downstream molecules, Akt and S6, and increased the levels of the proapoptotic molecule, cleaved PARP (poly (ADP-ribose) polymerase; Figure 2b), consistent with the decrease in cell viability. Furthermore, we also found that knockdown of *Aki1* discernibly induced apoptosis in PC-9, HCC827 and H1975 cells (Figure 2c).

We next assessed the effect of Aki1 inhibition, in comparison with EGFR inhibition, in *EGFR* mutant lung cancer cell lines. Like *EGFR* knockdown and erlotinib, *Aki1* knockdown considerably inhibited viability of PC-9 and HCC827 cells with exon 19 deletion in *EGFR*. In addition, *Aki1* knockdown inhibited viability of H1975 cells with exon 21 L858R and exon 20 T790M double mutations as potently as *EGFR* siRNA, whereas erlotinib had no effect (Figures 3a and b). These results suggest that targeting of Aki1 may be valuable for treating *EGFR* mutant lung cancer cells, especially with T790M gatekeeper mutation.

Aki1 knockdown inhibits tumor growth of lung cancer with EGFR T790M secondary mutation *in vivo*

Next, we examined the antitumor potential of *Aki1* siRNA against H1975 cells with *EGFR* T790M gatekeeper mutation *in vivo*. Intratumoral injection of either scramble or *Aki1* siRNA complexed with invivofectamine was performed on days 5 and 8. In a previous report, *MAGE-D1* gene knockdown by three direct injections of siRNA complicated with invivofectamine into the local region indicated 50% inhibition of protein expression.[26] *Aki1* siRNA treatment dramatically inhibited tumor growth in comparison with control or scramble siRNA (Figures 4a and b). We confirmed knockdown of Aki1 and the inhibition of downstream signaling molecule, S6, in tumors by western blotting (Figure 4c). These results clearly indicated the therapeutic potential of *Aki1* siRNA against lung cancer with *EGFR* T790M mutation *in vivo*.

Combined Aki1 and *EGFR* blockade strongly suppressed cell viability of lung cancer cells with *EGFR* T790M secondary mutation

Irreversible EGFR-TKIs and mutant selective EGFR-TKIs were developed to overcome *EGFR* T790M gatekeeper mutation-mediated resistance to erlotinib and gefitinib. Here, we examined whether Aki1 knockdown could augment the therapeutic efficacy of these new generation EGFR-TKIs. Irreversible EGFR-TKI, CL-387,785 and BIBW2992, and the mutant-selective EGFR-TKI, WZ4002, reduced the viability of H1975 cells, whereas erlotinib had no such effect. *Aki1* knockdown suppressed cell viability and further augmented the various dose inhibitory effects of CL-387,785, BIBW2992 and WZ4002 (Figure 5a and Supplementary Figure S4). Consistent with these findings, *Aki1*

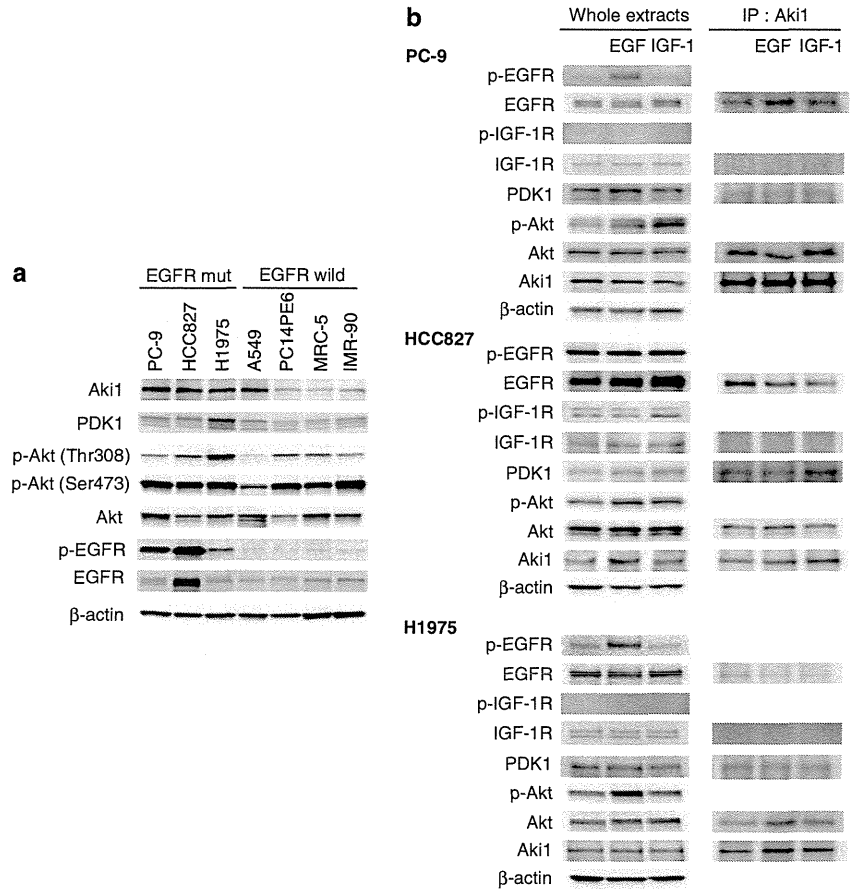

Figure 1. Aki1 expression and association to EGFR in EGFR mutant human lung cancer cell lines. (**a**) *EGFR* mutant human lung cancer cell lines (PC-9, HCC827 and H1975), *EGFR* wild-type human lung cancer cell lines (A549 and PC14PE6) and human lung fibroblast cell lines (MRC-5 and IMR-90) were lysed and the indicated proteins were detected by western blotting. (**b**) *EGFR* mutant lung cancer cell lines were treated with or without EGF (50 ng/ml) or IGF-1 (50 ng/ml) for 10 min. Then, cells were lysed and the indicated proteins were detected by western blotting with or without immunoprecipitation of Aki1.

knockdown decreased the levels of Akt and S6 phosphorylation, and increased the level of Par-4 and cleaved PARP, when combined with WZ4002 (Figure 5b). These results suggest the usefulness of *Aki1* knockdown combined with new generation EGFR-TKIs against lung cancer with *EGFR* T790M gatekeeper mutation.

Aki1 is frequently expressed in *EGFR* mutant lung cancer

We next examined Aki1 expression in 56 clinical specimens obtained from 56 lung cancer patients with *EGFR* mutation (Figure 6a and Supplementary Table S1). To confirm the specificity of the Aki1 by immunohistochemical staining, we performed Aki1 antibody absorption test by Aki1 peptide. The staining of Aki1 was remarkably diminished by pretreatment of sections with an Aki peptide at 4 °C overnight, compared with saline treatment, indicating the specificity of the antibody which we used for Aki1 staining (Supplementary Figure S6). Forty-two tumors were obtained from EGFR-TKI naive patients. Seven tumors were from patients who showed intrinsic resistance to the EGFR-TKIs, gefitinib or erlotinib. Another seven tumors were from patients who showed acquired resistance to EGFR-TKIs (Figure 6a). Of 42 EGFR-TKI naive tumors, the presence of Aki1 protein was scored as 2+ in 31 tumors (74%), 1+ in 8 tumors (19%), and – in 3 tumors (7%). Aki1 protein was detected diffusely in all of seven tumors with intrinsic resistance: 2+ in 4 (57%), 1+ in 3 (43%). Aki1 protein was detected diffusely in all of seven tumors with acquired resistance: 2+ in 6 (86%), 1+ in 1 (14%) (Figure 6a). Aki1 was detected in all tumors with acquired resistance, including four tumors with *EGFR* T790M mutation (Supplementary Table S1). These findings suggest involvement of Aki1 in EGFR-mediating signaling in lung cancer with *EGFR* mutations, including T790M gatekeeper mutation.

DISCUSSION

The results of the present study indicated that Aki1 constitutively associates with mutant EGFR even in the presence of EGFR-TKI. Silencing of *Aki1* induces apoptosis of *EGFR* mutant lung cancer cells, indicating that Aki1 has crucial roles in survival signal transduction in lung cancer cells with *EGFR* mutations. In a xenograft model, silencing of *Aki1* markedly inhibited growth of lung cancer cells with *EGFR* T790M gatekeeper mutation. Furthermore, Aki1 was frequently expressed in tumor cells of *EGFR* mutant lung cancer patients. Notably, it was detected in all tumors with acquired resistance to gefitinib or erlotinib, suggesting that Aki1 is an ideal target for *EGFR* mutant lung cancer, especially in cases with acquired EGFR-TKI resistance due to *EGFR* T790M gatekeeper mutation.

Although Aki1 associates with wild-type EGFR when activated by EGF,[25] it binds constitutively with mutant EGFR (Figure 1b).